International Journal of Biological Macromolecules 192 (2021) 999–1012

Contents lists available at ScienceDirect

International Journal of Biological Macromolecules

journal homepage: www.elsevier.com/locate/ijbiomac

Fabrication of stable electrospun blended chitosan-poly(vinyl alcohol) nanofibers for designing naked-eye colorimetric glucose biosensor based on GOx/HRP

Bilge Coşkuner Filiz [a,*], Yeliz Basaran Elalmis [b], İrem Serra Bektaş [c], Aysel Kantürk Figen [c]

[a] Yıldız Technical University, Metallurgy and Materials Engineering Department, İstanbul 34210, Turkey
[b] Yıldız Technical University, Bioengineering Department, İstanbul 34210, Turkey
[c] Yıldız Technical University, Chemical Engineering Department, İstanbul 34210, Turkey

ARTICLE INFO

Keywords:
Chitosan/polyvinyl alcohol
Electrospinning
Nanofiber
Glucose
Colorimetric
Biosensing

ABSTRACT

In this study, designing of a stable electrospun blended chitosan (CS)-poly(vinyl alcohol) (PVA) nanofibers for colorimetric glucose biosensing in an aqueous medium was investigated. CS and PVA solutions were blended to acquire an optimum content (CS/PVA:1/4) and electrospunned to obtain uniform and bead-free CS/PVA nanofiber structures following the optimization of the electrospinning parameters (33 kV, 20 cm, and 1.2 ml. h^{-1}). Crosslinking process applied subsequently provided mechanically and chemically stable nanofibers with an average diameter of 378 nm. The morphological homogeneity, high fluid absorption ability (>%50), thermal (<230 °C) and morphological stability, surface hydrophilicity and degrability properties of cross-linked CS/PVA nanofiber demonstrated their great potential to be developed as an eye-readable strip for biosensing applications. The glucose oxidase (GOx) and horseradish peroxidase (HRP) was immobilized by physical adsorption on the cross-linked CS/PVA nanofiber. The glucose assay analysis by ultraviolet-visible (UV–Vis) spectrophotometry using the same enzymatic system of the proposed glucose strips in form of absorbance versus concentration plot was found to be linear over a glucose concentration range of 2.7 to 13.8 mM. The prepared naked eye colorimetric glucose detection strips, with lower detection limit of 2.7 mM, demonstrated dramatic color change from white (0 mM) to brownish-orange (13.8 mM). The developed cross-linked CS/PVA nanofiber strips, prepared by electrospinnig procedure, could be easily adapted to a color map, as an alternative material for glucose sensing. Design of a practical, low-cost, and environmental-friendly bio-based CS/PVA testing strips for eye readable detection were presented and suggested as an applicable medium for a wide range of glucose concentrations.

1. Introduction

Various analytical methods for detecting glucose have been described, including electrochemical, fluorescent, and colorimetric [1–3]. Colorimetric biosensing techniques have attracted significant interest due to their favored properties, such as high selectivity and sensitivity, practical and straightforward use, and low cost [4,5]. High price and complicated instrumentations are not required in the colorimetric method, and analysis results can be obtained simply by naked eye observation owing to the color change. Furthermore, the colorimetric method is regarded as a potential method for clinical point-of-care and on-site detection [4,6]. Hydrogen peroxide (H_2O_2)-based colorimetric detection of glucose has been investigated based on several materials such as nanoalloys [7], nanofibers [3,8], nanosheets [9], and composite structures [10,11].

As a crucial carbohydrate in biological metabolisms, glucose has been stated as a double-sided molecule because of its physiological and pathological influences [12]. It plays an essential role in metabolic homeostasis, body functions and is also one of the foremost carbohydrate energy sources [1,13]. The close relation of glucose with the disorders of glucose metabolism and islet cell carcinoma makes it a substantial medical analyte [2]. Diabetes mellitus has become a global threat to human health since it is one of the leading reasons for morbidity and disablement [14]. It is considered one of the leading causes of heart illness, kidney failure, and aplasia [15]. Atypical blood glucose levels can be used as an identifier for all of these indications [12]. Thus, the

* Corresponding author: Yıldız Technical University, Metallurgy and Materials Engineering Department, İstanbul 34210, Turkey.
E-mail addresses: coskuner@yildiz.edu.tr, bilgecoskuner@gmail.com (B. Coşkuner Filiz).

https://doi.org/10.1016/j.ijbiomac.2021.10.048
Received 14 July 2021; Received in revised form 14 September 2021; Accepted 7 October 2021
Available online 13 October 2021

determination of blood glucose concentration levels is significant, particularly for diabetes patients [13]. The development of glucose sensors with high sensitivity, low cost, reliability, and remarkable selectivity has attracted increased interest in the food industry and the medicinal field [15].

Biological structures including enzymes, antigens, antibodies, and cells constitute the biorecognition components of biosensors. Using these various biostructures broad range of applications such as hazardous chemical detection and glucose detection are possible. Biosensors containing enzymes as biorecognition molecules are very specific, selective and allow detection precisely [16]. Most glucose biosensors for serum glucose detection rely on the glucose oxidase (GOx) enzyme and an accompanying peroxidase enzyme. GOx catalyzes the reaction where glucose substrate is oxidized with molecular oxygen co-substate to produce gluconic acid and H_2O_2. Subsequently, H_2O_2 is consumed by the peroxidase catalyzed reaction, where a colorless chromogenic agent is oxidized to produce a colored product allowing colorimetric detection [13,17,18].

Within the several types of nano-size materials, nanofibers synthesized via electrospinning process have been taken attention. Nanofibers have a large surface area, high porosity, and accessible functionalization properties that make them proper supports for several types of substrates [19]. Besides fiber production could be performed via several techniques such as wet-spinning [20], drawing [21], casting [22], etc. electrospinning is a low-cost and practical approach for obtaining these types of materials [23]. Their properties enlarge their application area from energy to biobased applications [23–25]. The usage of nanofiber in the biosensing application has been growing so fast due to these materials' effective results for bio-based sensing agents [26]. Various nanofibers in different compositions and morphology have been designed for colorimetric biosensing combined with the electrospinning process's advantage [27,28]. Li et al. used the electrospinning as an enzyme immobilization technique to develop optical fibers for glucose sensors. GOx-PVA solutions were prepared and used for the nanofibers alternative to a biosensor for glucose detection [29]. Puttananjegowda et al. demonstrated silicon carbide nanoparticles embedded electrospun nanofibrous membrane-based glucose sensor electrodes to improve materials properties [30]. Jiang et al. prepared hybrid nanofibers as a robust peroxidase-like catalyst for the sensitive colorimetric detection of ascorbic acid. His work offers a good relationship between 0-50 μM for ascorbic acid detection [31]. Dhawan et al. developed CS-PVA nanofibers for colorimetric point-of-care detection of cholesterol by immobilizing cholesterol oxidase and peroxidase enzymes on mats [32]. The usage of CS in the structure of blended nanofibers provides several advantages such as production of biodegradable, non-toxic material with good enzyme adsorption ability due to the interactions between its functional groups (amino and hydroxyl) and enzyme. The pristine CS in powder form has a low specific surface area without pores that leads to inefficient enzyme immobilization. Preparation of CS based nanofiber by a simple and well-known electrospinning technique has promising positive effects as large surface area to volume ratio, high porosity with interconnected voids, excellent mechanical behavior and durable structures which made them desirable structures to immobilize enzymes [33–35]. Preparation of nanofibers by use of electrospinning also enable the production of high purity surely that minimizes the contamination risk of the final product containing the enzyme [36]. However, using CS to prepare nanofibers has some limitations due to the structure of CS. It is impossible to spin CS without blending it with another polymer [35]. The enzyme is supported by physically binding with help of hydrophobic and van der Waals interactions with a simple experimental procedure [37].

In the modern era of science a large number of substances are required to be sensing in our World by new technologies together with several industrial and anthropogenic activities [38]. Nowadays research in the field of materials science enlighten us that many scientists are doing research on the several functionalized nanomaterials and composites for toxic ions sensing and/or removal such as glassy carbon electrode for amperometric uric acid detection [39] $Ag_2O@La_2O_3$ nanosheet probe for amperometric 3-methoxyanilinedetection [38], NBBSH/Nafion amperometric sensor for arsenic detection [40], 1-naphthylamine ligand based conjugate material for nitrite monitoring and removal [41], synthetic zeolites from bio-slag for cesium adsorption [42], crown ether based conjugate material for cesium removal [43], ligand based functional composite material for Pb(II) and Ni(II) capturing [44,45], $Co_3O_4@Er_2O_3$ nanorods for 4-hexylresorcinol amperometric sensing [46]. Owing to different methods such as electrochemical sensing methods in terms of amperometric [47–49], impedimetric [50–52] and naked-eye colorimetric [53,54] sensing methods have been reported for the determination of several different substance. The reported electrochemical methods are effective and sensitive yet they are very expensive and complicated. Together with this the naked eye sensing method is a good idea for the practical testing and sensing applications. In addition to the chemical sensing methods, the biological sensing technique based on use of enzymes provide low cost option. The use of supporting materials such as mats [55,56], beads [57,58], spheres [59], films [60,61] and immobilization of enzymes on supporting materials have to be performed for the preparation of test strips. Moreover, bio-based nanostructure materials are being good options due to being environmental-friendly, non-toxic, and easy-availability as enzyme supporting materials. Thus, many studies have been reported in which bio-polymer based nano-materials have been improved for the immobilization of enzymes.

CS is polycationic, thus the NH_2 groups are protonated at pH below the pKa of the amino groups via glucosamine residues (pKa 6.3). The higher the degree of deacetylation, the more amino groups are available to interact with and immobilize enzymes [62]. Between several options, chitosan–based nanofibers exhibited better physical adsorption capability compared to other physical forms such as powder, film etc. This characteristic has been ascribed to the material's enhanced surface area, which can improve protonated amino group availability through nanofibers and result in additional adsorptive sites [33,63]. Nanofibers have recently gotten a lot of attention for enzyme immobilization, not only because of their higher surface area to volume ratio and enzyme loading capacity, but also because of their higher chemical and mechanical stability, which is important for ensuring the support's physical resistance. Nanofibers do not have the disadvantages of nanoparticles, such as aggregation behavior, which can impact enzyme stability and function, and the need for extra operations (centrifugation or membranes) to separate nanocapsules. The nanofibers that have been gathered form a macrostructure of nanofibers that can be readily separated and reused [33,55,62,64,65]. Ji et al. prepared core-shell type hollow polyurethane based nanofiber membrane for glucose detection. They fabricated core-shell nanofibers by using co-axial electrospinning. GOx, HRP, and chromogenic agent (ABTS or o-dianisidine) were in-situ immobilized inside of the nanofiber structure [16]. In this work, with the purpose of naked-eye colorimetric sensing of glucose, test strips were prepared by post-immobilization of GOx-HRP on electrospun PVA-CS mats. The advantages of chitosan and nanofiber structure were combined to prepare naked-eye colorimetric glucose sensing strips. Novelties of our work compared to Ji et al. were (i) the usage of chitosan and PVA polymer solutions which were blended and electrospunned to get optimized nanofiber structures, (ii) application of GOx and HRP enzyme solutions for physical immobilization on the nanofiber surface, and (iii) application of glucose solution droplets on the surface and than the o-dianisidine as a chromogenic agent to get color intensity change. The novelty of this research also includes the fabrication of CS-PVA nanofibers by electrospinning to be used as naked-eye glucose detection medium based on cascade GOx and HRP enzyme system.

In the current work, crosslinked CS-PVA nanofibers were suggested as proper media for the immobilization of GOx and HRP enzymes for colorimetric glucose sensing. CS, which is a polysaccharide natural biopolymer was selected due to its stated features such as mechanical

Table 1
The compositions and electrospinning conditions of nanofibers.

Solution	Concentration, wt%		Mass ratio of CS/PVA	Spinning conditions		
	Chitosan	PVA		Applied voltage, kV	Collecting distance, cm	Flow rate, mL h^{-1}
PVA	–	10	0/1	25	7.5	1
CS/PVA-1	2.5	10	1/3	34.6	20	1.2
CS/PVA-2	2.5	10	1/4	33	20	1.2
C-CS/PVA-2	2.5	10	1/4	33	20	1.2

strength and film-forming capability. PVA was used to enable the electrospinning of CS efficiently. Thus, the goal of this research is the synthesis of CS-PVA nanofibers based on electrospinning, understanding the effect of crosslinking on the physical properties of CS-PVA nanofibers and developing a proper material for enzyme immobilization as well as suggestted the possible use of nanofibers for naked eye colorimetric detection of blood serum glucose levels. Since CS and PVA are biocompatible and eco-friendly materials and easy to blend, they are good alternatives for naked eye colorimetric biosensing using CS blended PVA nanofibers performed without auxiliary equipment.

2. Materials and methods

2.1. Materials

Chitosan (CS) powder with medium molecular weight (M_W: 190.000–310.000 Da, 75–85% deacetylated) and polyvinyl alcohol (PVA, $(CH_2CHOH)_n$) with an average molecular weight of 72,000 and hydrolyzation of 97.5–99.5% mol, were purchased from Sigma-Aldrich and Fluka, respectively. Acetic acid (CH_3COOH) and glutaraldehyde solution (GA, 50 wt% in H_2O) were from JT Baker and Sigma-Aldrich, respectively. Anhydrous D-(+)-glucose and o-Dianisidine were obtained from Fluka. Sodium phosphate dibasic heptahydrate (PBS, $Na_2HPO_4{\cdot}7H_2O$, Fluka), sodium phosphate monobasic dihydrate ($NaH_2PO_4{\cdot}2H_2O$, Merck), and sodium chloride (NaCl, Merck) were used in the preparation of phosphate-buffered saline (PBS). Glucose oxidase (GOx) from *Aspergillus niger* (EC 1.1.3.4, 145,200 unit/g, Sigma), and peroxidase from horseradish (HRP, EC 1.11.1.7, 150 U/mg, Sigma) were stored at −20 °C and +4 °C, respectively. All the commercial products were used as received without any pre-treatment in experimental studies—deionized water used to prepare aqueous solutions and in other experimental procedures.

2.2. Preparation of CS/PVA solution

The solely and blend solutions of CS and PVA were prepared as explained below. PVA was dissolved in distilled water under stirring at 90 °C for 2 h to form a homogeneous solution of 10 wt%. The PVA solution was cooled down to room temperature and stirring continued for 24 h. CS powder was dissolved in 2 vol% aqueous acetic acid solution at room temperature with moderate stirring to obtain 2.5 wt% homogeneous CS solution. The blend solutions of CS/PVA were prepared by mixing at different mass ratios of given amounts as 1/3 and 1/4 of CS and PVA solutions. Correspondingly, these blended solutions were numbered as CS/PVA-1 and CS/PVA-2. The blend solutions were continuously stirred for 24 h at room temperature. All solutions were stored in the refrigerator at 4 °C before the spinning procedure.

2.3. Analyses of electrospinning solutions

The viscosity, pH, and conductivity of the prepared solely and blend solutions were analyzed before fabrication of nanofibers using Fungilab Viscometer, WTW Inolab pH Level 1 pH Meter, and WTW Inolab Cond7110 Conductometer, respectively.

2.4. Fabrication of CS/PVA nanofibers

Nanofibers were fabricated via electrospinning procedure at room temperature using a plate-type collector covered with aluminum foil. The solely and blend solutions were injected using a 10 ml syringe needle using a pump whose flow rate was controlled. The collecting distance between the tip and collector was changed depending on the solutions. The process conditions were optimized based on the formation of the Taylor cone in the system. The operating and optimizing conditions of each solution were given in Tables 1 and 2. The nanofibers were collected at plate-type surfaces. The nanofibers were dried at room temperature and stored in a vacuum desiccator before the characterizations and further applications.

Crosslinking is a stabilization process that leads to a multidimensional extension of the polymeric chain resulting in network structure. Cross-linking enables robustness and resistance to heat, and improves polymers mechanically. This critical process provides insoluble and infusible properties to polymers [66]. The nanofibers were crosslinked by using a 2.5 wt% GA solution (Figs. 1 and 5). The pH value of the GA solution was adjusted to 4 by using 0.1 M HCl solution. The nanofibers were placed into the solution and crosslinked for 48 h in the desiccator. The nanofibers were dried at room temperature and washed with deionized water three times to remove excess GA in the structure. The nanofibers were dried under an open atmosphere at room temperature before the characterization.

2.5. Characterization

The morphological characterization (Fig. 2) of fresh and used nanofibers was performed via scanning electron microscopy (SEM, Zeiss evo® ls 10). The nanofibers were placed on to carbon band, and Au-Pd coating was applied to all samples before the analyses. The diameters of fibers to calculate average values and obtain histograms were measured by using software of the equipment. The average fiber diameters were calculated via taking images of different samples, and fiber diameters were randomly measured. The nanofiber's topography and surface roughness characterization Fig. 3 were identified via atomic force microscopy (AFM, Shimadzu SPM-9600) in tapping mode with a silicon tip. The 4 μm × 4 μm area with a 0.8 Hz scanning rate was used for the characterization.

The chemical structure in terms of chemical bonds and functional groups of each nanofiber were investigated using Fourier transform infrared (FTIR) spectroscopy (Perkin Elmer Spectrum 100 Fourier, Fig. 4) and micro-Raman spectroscopy (WITech alpha 300R, Fig. 6). The FTIR measurements were performed in the attenuated total reflectance (ATR) part of the device in the wavelength range of 4000 to 650 cm^{-1} with 1 cm^{-1} resolution and 4 scans. The Raman analyses were performed at 532 nm laser between the 3740–100 cm^{-1}.

The thermal behavior of nanofibers was characterized via thermogravimetric (TG) and differential thermogravimetric (DTG) analyses. The measurements were performed with the Perkin Elmer Diamond instrument, which was calibrated by using the melting points of indium (T_m = 156.6 °C) and tin (T_m = 231.9 °C) under the same conditions as used for the samples. Thermal analyses of samples were carried out under a nitrogen atmosphere at a heating rate of 10 °C min^{-1} to 1000 °C. The

platinum crucible was used in all measurements.

To use nanofibers, especially in biosensing applications, it is necessary to figure out their stability properties under heating and water. The stability was tested by the contact angle, in vitro biodegradation, the degree of swelling in PBS, and SEM analyses (Figs. 7 and 8).

In vitro biodegradation of nanofibers was determined based on the weight loss of sample in PBS solution by the well-known procedure [67]. The sample was cut into pieces and weighted (W_0). Then the samples were placed into a PBS solution with pH 7.4 at 37 °C for 21 days. The samples were removed from the solution, washed, and weighted (W_d) after vacuum drying at specific time points such as 7 days, 14 days, and 21 days. The in vitro degradation was calculated as given below:

$$\text{In vitro degradation}\ (D,\%) = [(W_0 - W_d)/W_0] \times 100 \quad (1)$$

The swelling degree of the crosslinked nanofibers was determined by PBS absorption by a well-known procedure [67]. The samples were cut into square pieces and weighted (W_d), then incubated at 37 °C in PBS solution with pH 7.4. The samples were removed, and excess water was wiped and weighted (W_W). PBS absorption calculated based on the equation as given below, which was also swelling degree:

$$\text{Swelling degree}\ (SD,\%) = [(W_w - W_d)/W_d] \times 100 \quad (2)$$

The contact angle of crosslinked nanofiber (C-CS/PVA-2) was measured by a water contact angle measurements system (Attention Theta Flex). 10 μl PBS droplet applied on the surface of samples, and then the water contact angle (WCA) was measured directly.

2.6. Colorimetric measurement of glucose

Colorimetric glucose measurement using the ultraviolet-visible (UV–Vis, Fig. 9) absorption method was used to investigate the colorimetric functioning of the GOx, HRP, and o-dianisidine systems. GOx (10 U/mL) and HRP (10 U/mL) solutions were prepared in PBS (0.01 M, pH 7.4) and mixed at a 1:1 ratio to obtain the working enzyme blend (GOx/HRP) solution with 5 U/mL GOx and HRP concentrations. 10 mM o-dianisidine solution was used as the colorimetric substrate. Glucose solutions used were in the 2.7–13.8 mM concentration range. Glucose standard curve was obtained using UV–Vis spectrophotometer (Scinco S-3100) with 1.25 mL PBS, 0.275 mL enzyme blend, 0.2 mL o-dianisidine, and 0.275 mL glucose solutions. The reaction started with the addition of enzyme blend, and the absorbance values of the test tubes were determined at 480 nm wavelength after 10 min of reaction time. The reaction of the colorimetric glucose detection assay is as follows:

$$\beta - D - \text{Glucose} + O_2 + H_2O \xrightarrow{GOx} D - \text{glucono} - 1,5 - \text{lactone} + H_2O_2 \quad (3)$$

$$H_2O_2 + o - \text{Dianisidine}_{(\text{reduced})} \xrightarrow{HRP} H_2O + o - \text{Dianisidine}_{(\text{oxidized})} \quad (4)$$

The colorimetric detection of glucose on C-CS/PVA-2 nanofiber was performed as follows. Nanofibers were prepared at 0.5 × 0.5 cm^2 dimensions for the immobilization of GOx and HRP enzymes. GOx/HRP blend solution used in the glucose detection with the spectrophotometric method also used to immobilize GOx and HRP enzymes on the nanofibers. 10 μL of GOx/HRP blend used in the immobilization process for 0.5 × 0.5 cm^2 sized nanofibers. The nanofibers dried at room temperature following the application of GOx/HRP immobilization and used to detect glucose in the concentration range of 2.7 to 13.8 mM. 10 μL of these glucose solutions applied to the nanofibers and incubated for 10 min and followed by 5 μL of o-dianisidine (10 mM) addition. The resulting color intensity was observed visually and related to the formed color gradient scale. Furthermore, 10 μL of PBS was applied instead of glucose solution on the prepared GOx/HRP immobilized nanofiber to serve as a control, keeping all other parameters as above stated.

3. Results

3.1. Analyses of electrospinning solutions

Several natural and synthetic polymers have been used for nanofibers synthesis via the electrospinning technique [68]. CS is a biodegradable, biocompatible, and non-toxic natural polymer in the form of saccharide. Since it is soluble in only acidic mediums such as formic or acetic acid, it can be hardly electrospinnable. The acidic media protonates the NH_2 group of saccharidic backbone to NH_3^+, and the structure becomes cationic polyelectrolyte. The electric field of the electrospinning system leads to positively charged groups. As a result of this, continuous fiber formation of chitosan can not occurred. Also, strong hydrogen bonding between NH_2 and OH groups determines chitosan solution properties. Both high and low concentrations of chitosan solutions do not have electrospinnable properties due to a high viscosity with three-dimensional structure at high concentrations and insufficient viscosity at low concentrations, respectively. To optimize the solution content and spinning procedure, polymer solutions in different content were prepared (see Table 2). Firstly, chitosan solution with 1 wt% concentration was prepared and aimed to spin, yet under various electrospinning condition the formation of Taylor cone could not be achieved. For this reason additives such as sodium chloride and ethanol were used in the content of the spin solutions to improve spinnability of the solution. Under different flow rate, tip to collector distance and voltage values, besides some content formed Taylor cone, it was not possible to get fibers in the collector plate. Different solutions have been investigated to get chitosan nanofibers based on electrospinning, such as blending with guest polymer or changing the solvent of chitosan solutions [69,70]. PVA is a synthetic polymer with mechanical durability and high solubility in water. Biopolymers generally have poor solubility, low strength and thermal stability. Blending the synthetic and biopolymer is an excellent alternative technique [67]. This approach enhances the properties of both polymers into one. The interaction between CS and PVA at the molecular level is due to hydrophobic side-chain aggregation and intermolecular and intramolecular hydrogen bonds [68,70,71]. For that reason, CS solutions were decided to be blended with PVA solutions until the Taylor cone was observed and fibers were formed, electrospinning parameters were tested for optimization. Two different blending ratio of CS and PVA were selected as 1/3 and 1/4 in which PVA content aimed to be higher due to low and high spinnability properties of CS and PVA, respectively. The solutions were spinned between the 20–35 kV applied voltage, 5–20 cm tip to collector distance and polymer flow rate settled to 1.2 mL h^{-1}. For each solutions, conditions were tested and optimized based on the formation of fiber as given in Table 2.

The pH, conductivity, and viscosity values of PVA, CS, and CS/PVA electrospinning solutions were analyzed individually to correlate the polymer's spinnability and properties. The pH values of solely PVA and CS solutions were measured as 5.65 and 3.95, respectively. Blending CS solution with PVA resulted in acidic CS/PVA-2 solution (pH: 4.50). The pH of the solution frivolously affects the formation of the fiber, despite it was adequate for the diameter of fibers. The low pH values-acidic mediums decreased the viscosity of the PVA solutions that affected the fiber structure [72]. The viscosity values of PVA and CS solutions were 1751 cp and 222 cp, respectively. The blended polymer solution CS/PVA showed a significantly higher value (3963 cp) than each solution. This incensement was in agreement with the literature. The blending of the PVA solutions with CS solutions led to increase viscosity due to the interaction between polymers, especially hydrogen bonds [73].

In the content of blend solutions of CS/PVA-2, ratios of polymers and as a result of total polymer concentrations changed. The interaction between PVA and CS polymers were resulted in chain entanglement of

Table 2
Optimization of solution and fiber parameters of electrospinnig solutions.

Solution	Flow rate, mL min^{-1}	Distance, cm	Voltage, kV	Formation of Taylor Cone	Spin of solution	Fiber formation	Optimized conditions
Filtered 1 wt% CS	0.5	5–20	25–30	–	–	–	–
	1.5	5–20	25–30	–	–	–	–
	2.5	5–20	25–30	+	–	–	–.
1 wt% CS + NaCl	0.5	5–25	25–27	+	+	–	–.
	1.5	5–25	25–27	+	+	–	–
	2.5	5–25	25–27	+	+	–	–
1 wt% CS + NaCl + EtOH	1.2	20	25	+	+	–	–
2.5 wt% CS	1.2	5–30	25	–	–	–	–
10 wt% PVA	1–1.5	5–30	15–35	+	+	+	1 $mL.h^{-1}$ 7.5 cm 25 kV
CS/PVA-1	1–1.5	5–30	15–35	+	+	+	1.2 $mL.h^{-1}$ 20 cm 34.6 kV
CS/PVA-2	1–1.5	5–30	15–35	+	+	+	1.2 $mL.h^{-1}$ 20 cm 33 kV

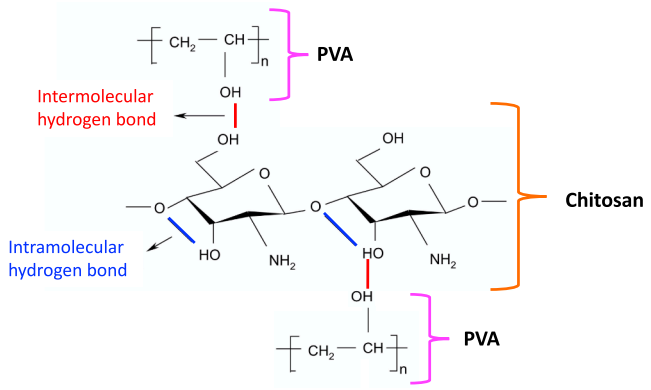

Fig. 1. The inter-and intramolecular interaction between the functional groups of PVA and chitosan.

polymers by intermolecular and intramolecular hydrogen bonding (see Fig. 1). This decreased the surface tension of the solution and enabled uniform nanofiber formation [74]. PVA is a hydrophilic and nonionic polymer with a 3D network structure of hydrogel polymer and can form hydrogen bonds and crosslinks with CS chains through hydroxyl groups. This also provides blending and formation of homogeneous solutions [75,76].

The conductivity values of pure and blend solutions were 1048 μS cm^{-1}, 3670 μS cm^{-1}, and 530 μS cm^{-1} for PVA, CS, and CS/PVA-2, respectively. The conductivity value of the solution is also an essential parameter for the electrospinning procedure. The formation of continuous jets during the spinning is required. The solutions with low conductivity and high viscosity enable higher resistance than a repulsive force that stretches the jet. That results in less charge transport by the jet and thicker fibers formation generally [77]. CS solution has a higher conductivity value due to water and detached acid molecules in acetic acid solution together polyelectrolyte nature of its solutions enables its spinning [78].

3.2. Characterization of fabricated nanofibers

Several spinning factors such as polymer concentration, viscosity, pH, conductivity, applied voltage, collection distance, and flow rate affect the formation of fibers [75]. Pure and different blends of PVA and CS solutions were prepared for that reason. CS is a hardly spinnable biopolymer that requires another polymer to overcome this problem. PVA shows favorable interaction with CS as a guest polymer, and as a result, this blended solution could be spinnable [70]. The solutions of PVA and CS/PVA-2 blends spun, and nanofibers were obtained after optimizing spinning conditions. The blended ratio of CS to PVA is essential due to the spinnability of the solution.

The SEM images and histograms of the nanofibers are given in Fig. 2. Pure solution of PVA and its blend solutions with CS synthesized bead-free uniform fibers. The PVA nanofibers showed a uniform diameter with a smooth structure. The diameter distribution illustrated in the inset of Fig. 2b is mainly 215 nm. Blending CS solution with PVA helped overcome beading, which is generally formed due to insufficient stretching of filaments during the bending of polymer solution jet [75]. Also, blending improved the spinnability of the CS solution. The addition of CS solution into PVA showed a significant effect on the nanofiber diameter, yet the smoothness and beadles morphology of the nanofibers still present. The average diameters and diameter distributions increased up to 245 nm and 378 nm. Besides the higher PVA concentration in the blend resulted a higher diameter, the nanofibers formed more separated. Lower PVA concentration led to crossover points in the structure of CS/PVA-1 nanofibers. For that reason, CS/PVA-2 was selected for further studies and crosslinked by the use of GA. There was a noticeable change observed after the CS/PVA-2 was crosslinked. The bead-free, uniform, and fine morphology of nanofibers were not destroyed during crosslinking with GA. The histogram (see inset of Fig. 2h) shows that diameter did not alter from the crosslinking process.

AFM analysis was used to demonstrate the surface morphology of fabricated nanofibers. The tapping mode could decrease the irreversible destruction of the surface in 3D structure. The 3D morphologies of the 4 μm × 4 μm area of the fibers were shown in Fig. 3. The color intensity shows the vertical profile of the surface of the nanofibers. The light blue regions belonged to the highest points, and the dark blue regions have belonged to valleys. The surface roughness of nanofibers was analyzed via software. The average geometric roughness (R_a) of PVA, CS/PVA-2, and C-CS/PVA-2 was 4.53 nm, 58.123 nm, and 5.94 nm, respectively. Also, the root-mean roughness (R_q) of PVA, CS/PVA-2, and C-CS/PVA-2 were 5.34 nm, 58.99 nm, and 6.96 nm, respectively. Blending the PVA with CS increased the surface roughness value of nanofibers. Crosslinking process created a softer and smoother surface compared to CS/PVA-2. However, the roughness of C-CS/PVA-2 nanofiber was higher than the roughness of PVA nanofiber. Increased roughness results in improved wettability and interfacial bonding by providing more extended surface area [79].

The molecular and functional group characterization for chemical structure determination and clarification of polymer interactions was carried out using FTIR (see Fig. 4a) and Raman (see Fig. 4b) techniques. The pure CS functional structure was characterized by FTIR technique. In the infrared spectrum of CS, the characteristic peaks were observed in agreement with the literature. N—H_2 and O—H stretching vibrations

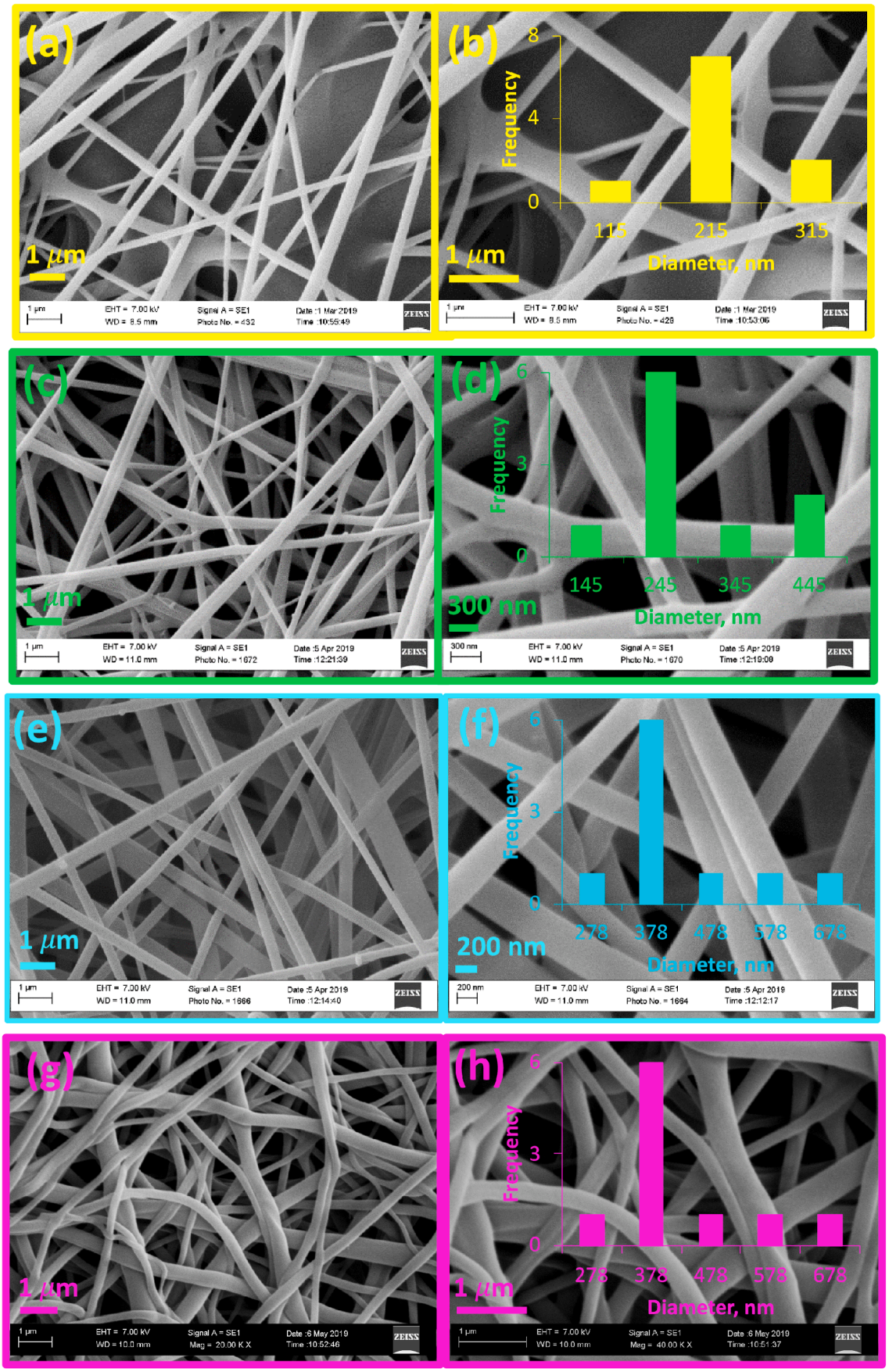

Fig. 2. SEM micrographs of nanofibers: (a, b) PVA, (c, d) PVA/CS-1, (e, f) PVA/CS-2, (g, h) C-PVA/CS-2. Insets show the histograms of individuals.

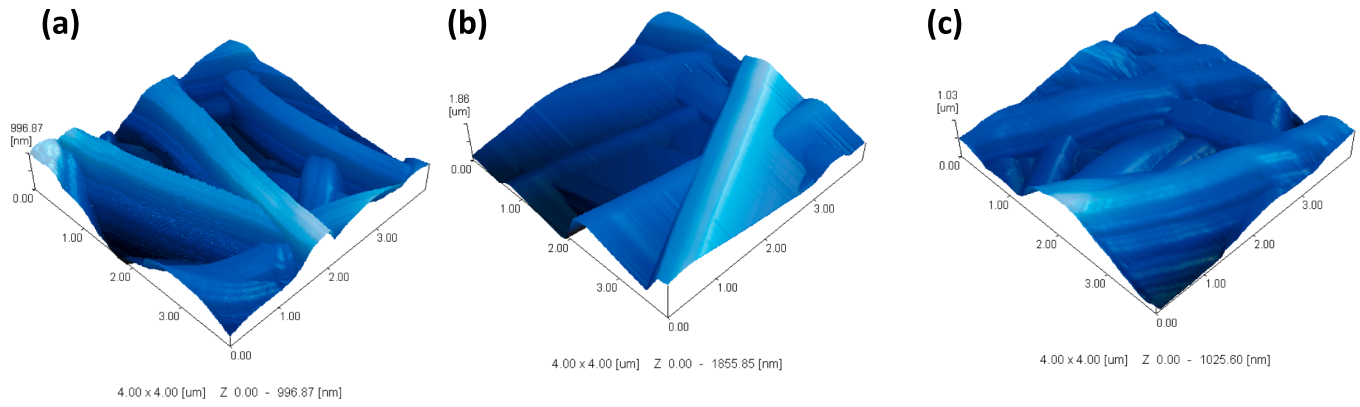

Fig. 3. 3D AFM images of nanofibers: (a) PVA, (b) PVA/CS-2, (c) C-PVA/CS-2.

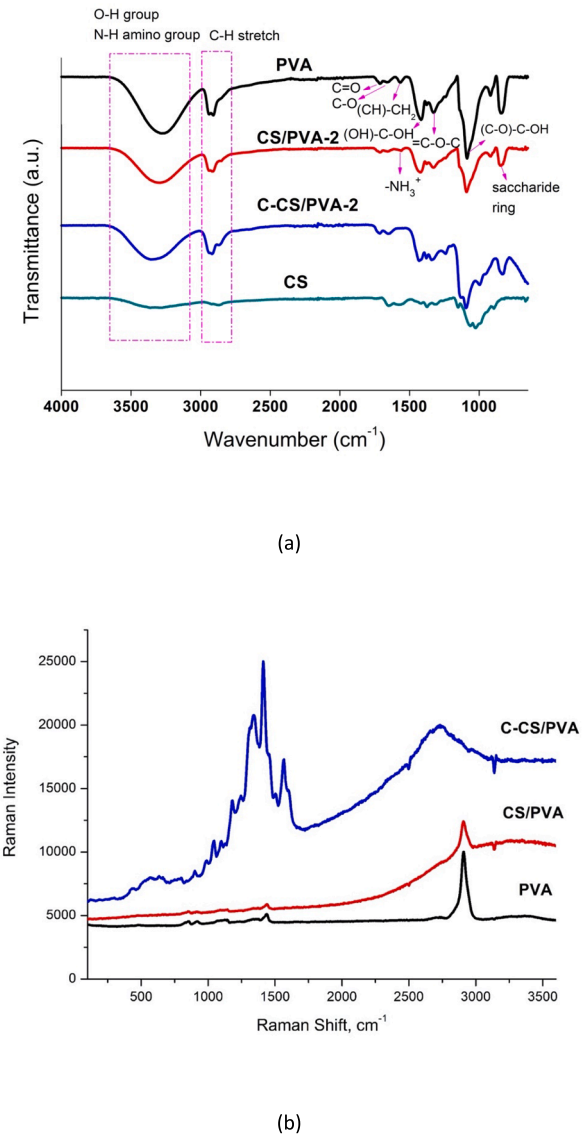

Fig. 4. FTIR spectrum of CS powder, PVA, CS/PVA-2 and C-CS/PVA-2 nanofibers (a) and Raman spectrum of PVA, CS/PVA-2 and C-CS/PVA-2 nanofibers (b).

presented a broad peak at 3365 cm^{-1}. The peak related with C—H_2 observed around 2860 cm^{-1}. In addition, the bands about 1650 cm^{-1} and 1565 cm^{-1} were assigned to C═O vibrations of amido I and N—H of amide I. The C—N stretching bands were presented at 1373 cm^{-1} and 1308 cm^{-1}. The C—O deformation of hydroxyl groups was detected at 1065 cm^{-1}. The vibrations of C—O and C—O—C related with saccharide structure were observed below 1025 cm^{-1} [70,80].

The FTIR spectrum of pure PVA nanofibers presented abroad peak related with O—H stretch from the intermolecular and intramolecular hydrogen bonds at 3278 cm^{-1}. Peak detected at 2909 cm^{-1} assigned to C—H stretch of alkyl groups. At the range of 1700–1699 cm^{-1}, peaks related with C═O and C—O stretches of the remaining acetate groups in PVA were recorded [71]. Wagging vibrations of the CH band showed a peak at 1424 cm^{-1}. The coupling of OH in-plane vibrations was observed at 1326 cm^{-1} [77]. The peak at 1086 cm^{-1} was assigned to bending OH groups of alcohol and stretching of C═O [81].

The FTIR spectrum of CS/PVA-2 nanofiber mats presented characteristic peaks related to PVA, CS, and their interaction. Due to the inter- and intramolecular interaction between the PVA and CS, ionization of the primary amino groups (—NH_3^+) of chitosan was detected at about 1550 cm^{-1}. Bands of C═O stretching vibrations were observed at about 1700 cm^{-1}, related to the vinyl acetate residues in PVA and acetyl group residues in CS [70,73,82]. The characteristic peaks of chitosan were observed at 1090 cm^{-1} and 844 cm^{-1} related to the saccharide structure of a repeated unit of CS. Also, the double absorption bands overlapping conditions with broad peaks related to N—H symmetrical vibration due to amine group of CS and O—H stretching of PVA seen at 3295 cm^{-1}. Similar to PVA at 2916 cm^{-1}, C—H stretching was indicated [73].

The Raman spectrum of PVA, CS/PVA-2, C-CS/PVA-2 were given in Fig. 4b. As can be seen from spectrums of Raman scattering, PVA and chitosan showed their characteristic bands. The spectrum of solely PVA nanofiber sample recorded a band with a maximum at 2853 cm^{-1} that can be attributed to valence C—H vibrations, a band at 1459 cm^{-1} to the shear mode, a characteristic peak of PVA. Also C═O groups which were due to the un-hydrolyzed groups of PVA, were recorded in the spectrum of PVA [83]. Similar to this pattern, CS/PVA nanofiber, which was prepared from the blend solutions of PVA and chitosan, also showed characteristic peaks related to epoxy C—H stretching of chitosan at 2923 cm^{-1}. Stretching vibrations related to the ring also recorded bands between 900 and 1350 cm^{-1} [84].

The formation of strong bands at about 1600–1100 cm^{-1} showed the crosslinking of PVA and CS polymers. The band formed at 1559 cm^{-1}, assigned to the $_{\nu}$(C═N) mode, was characteristic for the formation of the imine group due to covalent crosslinking. The peak observed at 1415 cm^{-1} was related to $_{\delta}(CH_2)$. The band's formation at 1347 cm^{-1} associated with $_{\nu}$(C—N—C) mode related to crosslinking due to chemical bond formation between GA and CS. The bands recorded at 2739 cm^{-1},

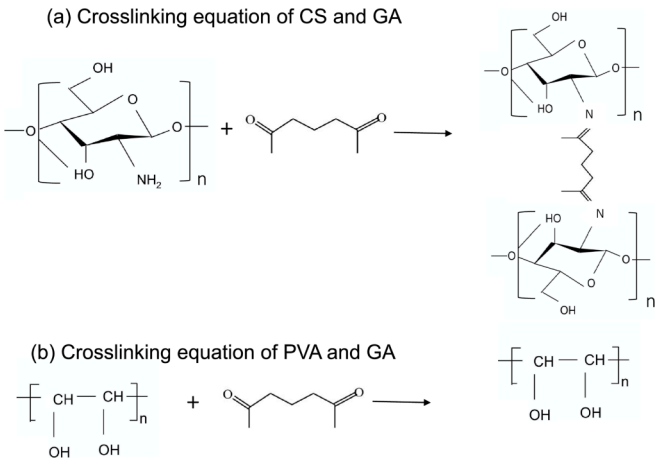

Fig. 5. Crosslinking mechanism of CS-GA (a) and PVA-GA (b).

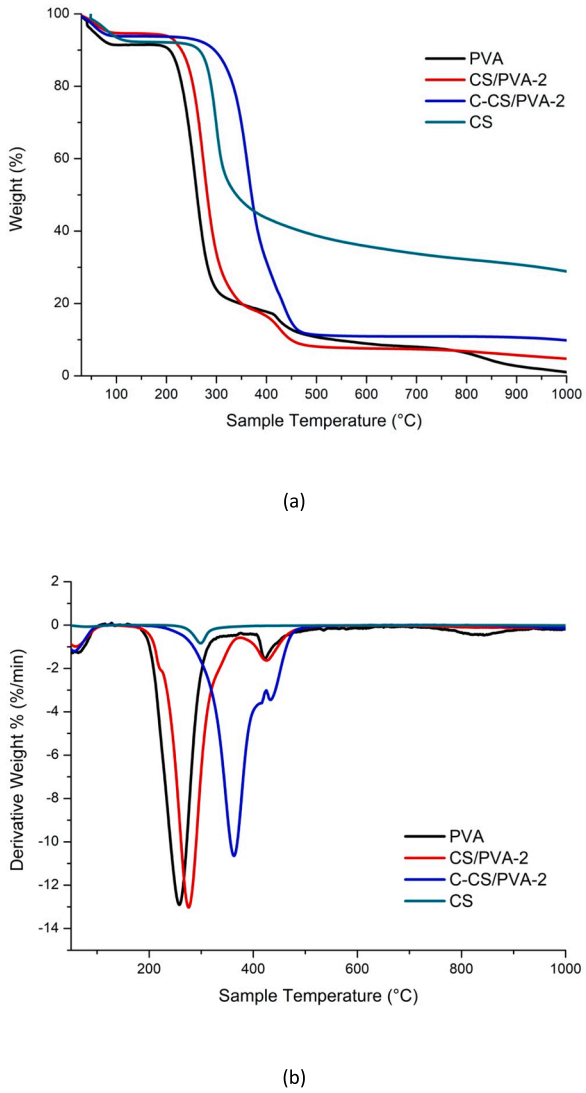

Fig. 6. TG (a) and DTG (b) curves of CS powder, PVA, CS/PVA-2 and C-CS/PVA-2 nanofibers.

1183 cm^{-1}, 1049 cm^{-1}, and 586 cm^{-1} were assigned to vibration of C—O, C—C, and δring [85]. The crosslinking process occurred between aldehyde groups of GA and some amine groups of CS, and the imine groups could also be formed (see Fig. 5). Crosslinking was confirmed from the peaks at about 1660 cm^{-1} in the spectrum of C-CS/PVA-2. As seen from the spectrum of crosslinked fibers functional groups related with CS and PVA were still relevant. Moreover, the crosslinking process of both polymers by using GA might form the same functional groups [84].

TG and DTG analyses could provide valuable information about the thermal behaviors of nanofibers (see Fig. 6). The thermal degradation behavior of pure CS was also given. As can be seen from Fig. 6a and b, CS shows two degradation steps up to 1000 °C. The first degradation was related with evaporation of the residual moisture (8 wt%) present in its structure that finalized about 125 °C. The second stage belongs to the decomposition of polymeric structure of CS. The decomposition rate of pure CS was maximized at about 300 °C, where the total weight loss was determined as 72 wt% [86]. Thermograms of PVA and CS/PVA-2 nanofibers exhibited three regions related to weight loss up to 1000 °C. The first region (up to 105 °C) corresponded to a loss of moisture maintained in nanofibers' structure. Pure PVA nanofibers contained about 8.5 wt%, and CS blended PVA nanofibers were about 5.5 wt% moisture. The degradation quantity of the first region was higher than the others due to the moisture, along with some volatile residues such as alcohols in the PVA structure [77]. The crosslinking did not affect the humidity content of nanofibers. The second region of decomposition showed drastic weight loss. After this step up to 180 °C, PVA nanofibers showed thermal stability. This temperature increased to 200 °C for CS/PVA-2 sample. Crosslinking of CS/PVA-2 nanofibers improved the thermal stability, and 50 °C incensement of thermal stability was obtained. The C-CS/PVA-2 nanofibers started to decompose at about 230 °C in the second degradation step. The thermal decomposition of polar groups, polyacetylene structure, and polymer dehydration occurred up to 375 °C with 76 wt% for CS/PVA-2. The second reaction was finalized at about 320 °C with 70 wt% weight loss for pure PVA nanofibers. This decomposition step accelerated at 260 °C and 275 °C for PVA and CS/PVA-2, respectively. The third step occurred at 425 °C with a smaller peak for PVA and CS/PVA-2 nanofibers. For the crosslinked CS/PVA-2 nanofibers the second degradation detected between 230 °C–480 °C with total of 82 wt% loss. Besides the other two showed separated peaks, decomposition of the crosslinked fiber accrued in one step. These reactions belonged to the decomposition of PVA and CS polymer chains that released CO_2 and other oxides [76]. The total weight loss of pure PVA was 99.22 wt%. As the CS was added to the structure, total weight loss decreased to 95.35 wt%. Crosslinking has a positive influence on the thermal stability of the nanofibers. The initial thermal degradation temperature is stated at a higher temperature. With this, low total mass loss (89.99 wt%) of nanofibers was observed after the crosslinking.

The stabilization of nanofiber structure is essential for chitosan-based materials to prevent solubilization of CS because of the net charge under its salt forms [87]. In this study, CS/PVA-2 nanofibers were stabilized by crosslinking via GA. The stability of the nanofibers was tested by in vitro biodegradation, swelling tests, contact angle, and SEM for biosensing application.

In this study, the PBS immersion method was used for the biodegradation experiments. According to the biodegradability results, CS/PVA-2 nanofibers were directly dissolved in PBS solution. The degradation process contained solvation and depolymerization mechanisms that lead to loss of polymer helpful physicochemical properties. In vitro biodegradation results of PVA and C-CS/PVA-2 nanofibers were given in Fig. 7a. As could be seen from Fig. 7a, crosslinked nanofiber C-CS/PVA-2 was much more slowly degraded compared to PVA. This was due to the chemical crosslinking between GA and amine groups of chitosan. Crosslinking of polymer nanofibers caused slower depolymerization of the structure and enhanced the stability against PBS solution. Also, it

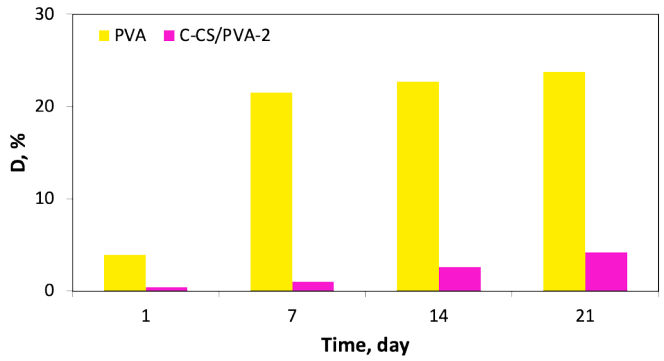

(a)

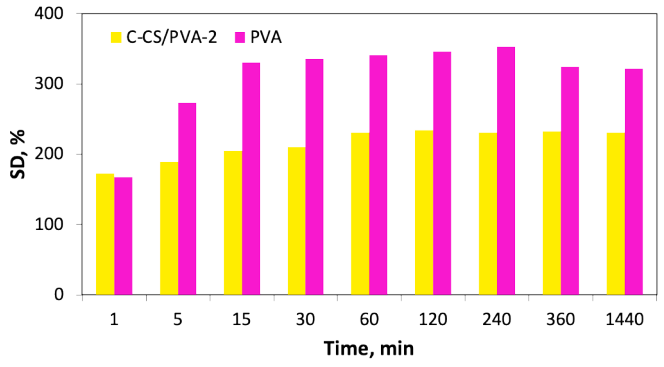

(b)

Fig. 7. In vitro degradation (a) and swelling degree (b) results of PVA and C-CS/PVA-2 nanofibers.

was evident that blending CS with PVA and crosslinking decreased the degradation rate of the polymer. Also, a higher density of crosslinking between amine groups of CS and GA than hydroxyl groups of PVA led to slower depolymerization and less degradation [68].

Fig. 7b shows the PBS swelling degree of PVA and C-CS/PVA-2 nanofibers. As revealed from the graphs, crosslinking and blending CS with PVA decreased the absorption efficiency compared to the solely PVA. Fig. 7b shows the PBS swelling degree of PVA and C-CS/PVA-2 nanofibers. As revealed from the graphs, crosslinking and blending CS with PVA decreased the absorption compared to the solely PVA as expected. PBS uptake of both PVA and C-CS/PVA-2 nanofibers was stabilized at the 30th minute. However, PVA nanofibers showed almost 50% higher PBS uptake when compared to the C-CS/PVA-2 nanofibers. Reduced swelling degree with the addition of CS is in agreement with studies previously reported. This result was due to the addition of CS that reduced the hydrophilic groups of PVA in the C-CS/PVA-2 mats via intermolecular interactions [74]. Although crosslinking of nanofibers allows the structure maintenance in aqueous media, crosslinking decreases the swelling of nanofibers depending on the increased inter-/intra-molecular interactions, which lead to increased network rigidity [88].

The fluid absorption ability is an essential parameter for nanofibers produced for strip-type biosensors. An ideal strip-type biosensor has to easily absorb the sample dropped on its surface. The contact angle measurement result showed hydrophilicity of the material. As shown in Fig. 8a, the contact angle of C-CS/PVA-2 was measured below 80°, proving the hydrophilic nature of nanofibers. The hydrophilicity of C-CS/PVA-2 indicated was the property of nanofibers to be used as a biosensor [68]. After 5 s of waiting, the fluid was adsorbed by

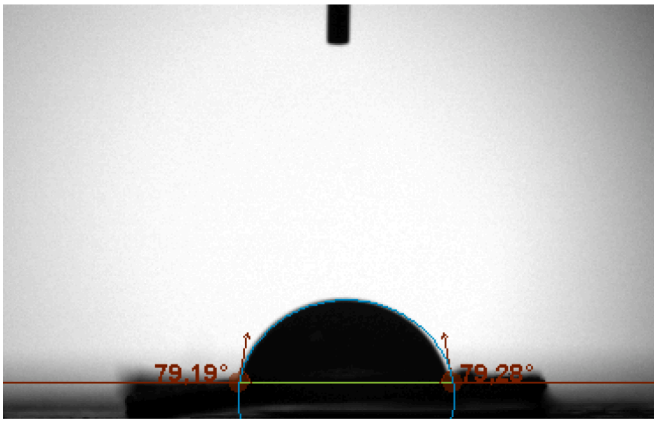

(a)

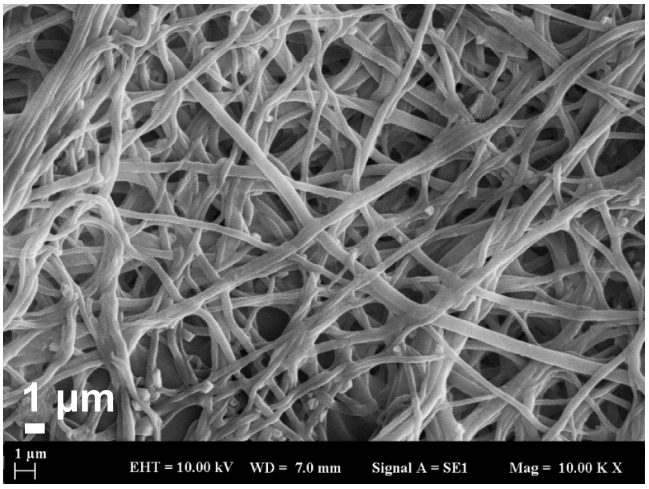

(b)

Fig. 8. The contact angle image of C-CS/PVA-2 nanofibers (a) and SEM image after test.

nanofibers. To evaluate whether the morphological stability of C-CS/PVA-2 nanofibers after PBS dropping was preserved, fibers were analyzed via SEM technique. As shown in Fig. 8b, nanofibers maintained their initial nanofiber forms with a 310 nm average diameter. SEM results indicated that crosslinking provided a mechanically stable nanofiber structure even after contacting with PBS solution.

It might be noted that the blending ratio of polymers, spinning conditions and crosslinking process affected the morphological properties in terms of fiber diameter, surface roughness and smoothness. The blending ratio of CS and PVA effected the intermolecular interaction between the functional groups and improved the spinnability of the polymer blends. A comparative investigation of CS/PVA and cross-linked CS/PVA nanofibers (378 nm) obviously showed that cross-linking process had a positive effect on the thermal, morphological and PBS degradation stability of the nanofiber mats. The thermal stability temperature of the cross-linked CS/PVA nanofibers was determined up to 230 °C, which was 200 °C for CS/PVA nanofibers. The high solubility problem was resolved by cross-linking process. Moreover this, surface roughness of cross-linked mat (6.96 nm) was enhanced compared to solely spinned fibers (5.34 nm). All results showed that, strip in the form of nanofiber was successfully developed for use of enzyme immobilization, showed resistance to environmental factors for

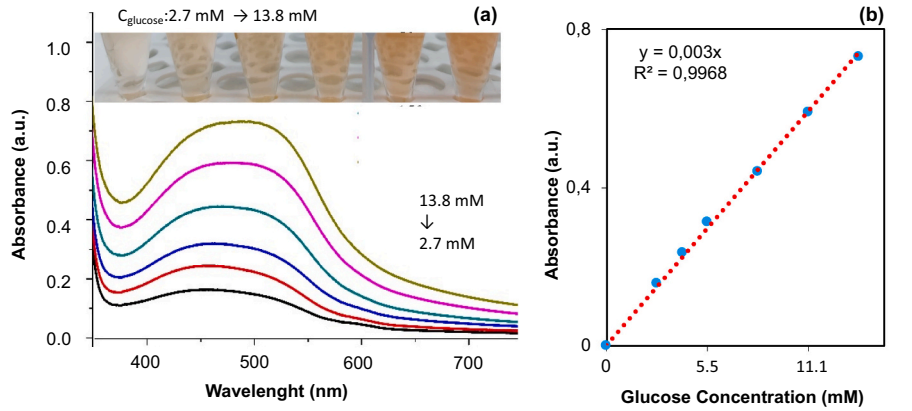

Fig. 9. UV–Vis. spectra of oxidized o-dianisidine depending on the glucose concentration in the presence of GOx and HRP (a) and a calibration curve of glucose (b) and the color changes as glucose concentration increased with a various concentration on C-CS/PVA-2 nanofibers (c).

biosensing conditions, that demonstrated it was a suitable material for glucose biosensing applications.

3.3. Colorimetric detection of glucose

To investigate the colorimetric assay performance of the GOx, HRP, and o-dianisidine system for glucose concentration measurements, GOx-HRP enzyme blend was included in the solution containing glucose and o-dianisidine, and developed brown color, which was due to the oxidation of reduced o-dianisidine, was measured at 480 nm wavelength after 10 min of incubation. Color reaction linearity was validated using glucose solutions with concentrations in the 2.7–13.8 mM range. UV–Vis spectra and the calibration plot obtained in the range of 2.7–13.8 mM glucose concentrations are presented in Fig. 9a and b. Response of the color reaction in this concentration range was found to be linear (R^2 of 0.9968) and specified the concentration-dependent behavior of the reaction. This result indicated that colorimetric enzyme assay could be utilized as a rapid and straightforward glucose detection method in the above-stated glucose concentration range.

In order to test the performance of enzyme immobilized C-CS/PVA-2 nanofibers for glucose sensing, experiments were carried out using glucose concentrations between 2.7 mM and 13.8 mM. A control test was also carried out using PBS instead of glucose solution. As shown in Fig. 9c, eye-readable color changes could be observed clearly from white to brownish-orange on the C-CS/PVA-2 nanofibers test strip. The intensity of the color changes on C-CS/PVA-2 nanofibers was concentration-dependent and sensitive to H_2O_2 concentration.

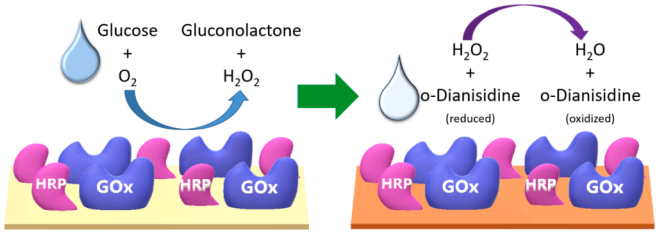

Fig. 10. Schematic description of the bi-enzyme reaction for glucose detection.

Colorimetric detection of glucose is based on the GOx catalyzed glucose oxidation by molecular oxygen, which results in the formation of gluconolactone and H_2O_2 [16,89]. The H_2O_2 then serves as the HRP substrate and is used in the oxidation of colorless o-dianisidine chromogenic substrate leading to a measurable colored product [2,16]. By dropping of glucose solution on C-CS/PVA-2 nanofibers strip, glucose molecules adsorbed on the surface of nanofibers. Then peroxide molecules (H_2O_2) are generated by their reaction with the immobilized GOx (see Fig. 10). The generated peroxide molecules might be stabilized by nanofiber and contributed to detecting the strip's ability leading to the oxidation of o-dianisidine to create a drastic color change.

In this study, GOx/HRP and the o-dianisidine system were first optimized and validated for glucose concentration dependence using the spectrophotometric glucose assay method. Then this system was applied on nanofibers for eye-readable glucose detection. Colorimetric results obtained were in sufficiently good agreement (Fig. 9a inset image and Fig. 9c). Tested glucose concentrations were between 2.7 mM and 13.8 mM, which cover the standard glucose detection requirement in the serum of humans that is between 3.9 mM and 6.4 mM [16,90]. As could be seen, the colorimetric biosensor obtained maintain its linear behavior at relatively higher glucose concentrations. According to these results, GOx and HRP loaded C-CS/PVA-2 nanofibers could be applied as glucose biosensors for practical glucose detection. Analytical results obtained in this study compared with some studies were reported in literature (Table 3). Although the glucose biosensors have been investigated, there are limited studies on the utilization of nanofibers for

Table 3
Comparison of some glucose detection studies reported.

Material	Detection technique	Linear range	Reference
Au/PPyNFs	Amperometric	0.2 mM to 13 mM	[47]
Nylon 6,6/4MWCNT fibers	Amperometric	0.01 mM to 2 mM	[91]
NiO-Ag NFs/GCE	Amperometric	up to 2.63 mM	[48]
NiCF nanofiber composite	Amperometric	2 μM to 2.5 mM	[49]
Electrospun CuCo-CFs	Amperometric	0.02 mM to 11 mM	[93]
Functionalized single-walled carbon nanotubes/ polypyrrole composites	Amperometric	0.02 mM to 6 mM	[94]
3D-NPZnO/chitosan	Impedimetric	1.0 mM to 18.0 mM	[52]
FTO/Nano-CuO/Chitosan/GOx	Impedimetric	0.2 mM to 15 mM	[51]
NiO thin film	Impedimetric	0.20 mM to 4.0 mM	[50]
Polyurethane hollow nanofiber membrane	Colorimetric	0.1 mM to 50 mM	[16]
Iridium(III) bis(2-phenylbenzothiozolatoN,C2′) acetylacetonate [(bt)2Ir(acac)] fibrous membran	Colorimetric	3.0×10^{-7} mM to 0.13 mM	[95]
Crosslinked chitosan/PVA nanofibers	Colorimetric	2.7 mM to 13.8 mM	This study

glucose detection using several detection techniques. In electrochemical techniques, conductive metal or polymers are used to develop biosensors for glucose detection in the range of 0.001 and 13 mM [47,48,91]. In the case of amperometric techniques, nanofiber materials have almost the same structure and detection range of 2 μM to 11 mM [49,92,93]. Colorimetric detection performance shows that nanofiber-based glucose sensing may be an alternative to other techniques, especially in application limits.

The naked-eye detection is based on variations in color intensity or tonality that's why it has higher limits of detection compared to the traditional instrument-based methods since, small changes in color tonality are difficult to notice by naked eye. As a result, only samples that show clearly discernible color changes when compared to control samples are regarded above limit of detection. Together with this, naked-eye detection provide advantages compared to classical methods which is generally unnoticeable with eye. Even though classical plate readers and spectrophotometers need large volumes of sample to detect the quantifying signal, a very little volume of sample is enough to change the color and achieve the detection with naked eye. The universal approach for "naked-eye based colorimetric sensing method" is defined as a small volume of substrate addition during the enzyme reaction which leads to enhancement in the colorimetric signal. The colorimetric signals can be recorded by taking photo with mobile phones or observed with naked-eye [96]. Several researchers have been used this method for the detection of analytes such as pesticide [97,98], rhodamine B [99], lysozyme [100], salivary glucose [101], mercury [102], and glucose in urine [103]. The clinical results using spectroscopic techniques have reported values around 4.1–5.5 mM for healthy person and 5.5–8.3 mM for diabetic person, including values as high as 8.3–13.8 mM for uncontrolled diabetic patients. The naked-eye color scale was improved based on the human blood sugar regions which was between the 2.7 mM–13.8 mM in this study. The lower naked-eye detection limit was 2.7 mM which defined as hypoglycemia level. The lower limit of the detection of naked-eye colorimetric sensor is defined as the low intensity color detectable by human eye or mobile phone camera [101]. Based on these concentration limits, the stirps were developed for the detection of glucose. Fig. 9 illustrates the visual colorimetric scale in the 2.7 mM−13.8 mM glucose concentration range for the developed C-CS/PVA nanofiber based test strips, obtained 10 min after the application of solution droplets. The obtained color intensity change as given in Fig. 9 could be used as semiquantitative scale for detecting glucose concentration. This procedure could be visually practiced with "naked eye" without use of extra spectroscopic equipment. As it was reported in the literature, the real blood sample was pre-treated to get serum [104]. Color scale was arranged according to the real blood glucose limits, thus pre-treatments such as centrifugation or filtration of blood samples to get serum, and incubation at room temperature will be enough for the use of proposed strips to detect glucose in real samples.

"Rapid detection method" is a simple and quick test technique which gives result in a short time [96,100]. Researchers have been improved several materials with different properties for the detection of glucose; Gao et al. prepared pH-responsive silica nanoparticles with detection time of 15 min [105]; Wu et al. synthesized Au NPs based synthetic cyclic peptide with detection time of 10 min [106].

In our study, cascade approach was preferred for the detection of glucose. The visual detection of glucose occurred in two subsequent steps; firstly glucose and GOx were reacted in PBS at room temperature where H_2O_2 was produced then HRP oxidized the o-dianisidine by the use of H_2O_2 resulting from the first reaction, in which the color intensity change could be observed by naked-eye. In the cascade reactions, if both reactions occur at almost same reaction rates, then the overall reaction rate is decided by how fast the H_2O_2 intermediate can react with HRP. As a result, when the distance between GOx and HRP is shortened, the overall reaction rate is projected to increase [107–110]. Also, the accumulation of H_2O_2 and glucolactone could result in degradation of GOx, yet by use of HRP in the bienzymatic system, H_2O_2 produced by glucose consumption of GOx is catalyzed into water and oxygen that eliminates this problem. As a result, a glucose sensor based on coupled GOx and HRP catalysis can have a wider sensitivity range and longer lifespan, because local oxygen concentrations will be partially replenished and the rate of enzyme degradation will be slowed due to the conversion of hydrogen peroxide before it attacks the GOx [111]. For that reason, we co-immobilized GOx and HRP enzymes on the surface of C-CS/PVA nanofiber strips. Several cascade reactions were carried through this approach [112,113]. So the formed H_2O_2 was directly in-situ reacted with HRP and o-dianisidine to give a color change. Several control experiments were performed to check and optimize the reaction time (10 min) based on the color change of chromogenic agent o-dianisidine due to the stability of the system with H_2O_2.

4. Conclusion

In this study, it was aimed to develop and characterize electrospun bio-composite CS and PVA blended nanofiber mats for the preparation of test strips, and to investigate the applicability to naked-eye readable glucose detection. By controlling the spinning parameters, reproducible fibers with nanoscale dimensions were obtained, and stable strips for particular demands and practical use were achieved via crosslinking. The developed strip-type composite nanofibers were successfully characterized and applied to naked-eye detection of glucose. 1:4 blend of CS (2.5 wt%) to PVA (10 wt%) solution was successfully electrospun (33 kV, 20 cm, 1.2 $mL.h^{-1}$) and subsequently crosslinked using GA to get crosslinked nanofibers (378 nm). The lower detection limit of stirps was arranged considering the lower human fasting blood glucose level (2.7 mM, 50 mg/dL) and colorimetric scheme was formed according to these limits. The experimental results indicated that crosslinked CS/PVA

nanofiber strips were good carriers for the stabilization of enzymes on their surface and provided homogeneity to achieve a highly effective and stable structure for glucose detection. Moreover, the composite material showed high naked-eye glucose detection performance, and indicated the bio-composite material content and electrospinnig technique as a promising economic, and environmental friendly material and technique for glucose detection. Thus, this work suggests that CS based nanofiber strip is applicable for biosensing applications of glucose due to its homogeneity to achieve a highly effective and stable structure. It is also worth that this present work demonstrated the usage of environmental friendly electrospinning solution and also the crosslinking agent and integrated them to provide stable fibers. Although the polymer, solvent, and crosslinking agents used in the production of nanofibers are all environmental friendly and degradable, environmental friendly material with low biodegradability has been prepared with the applied electrospinning crosslinking procedure. The main advantages of the method were easy to use with simplicity, the ability to rapidly attain phase equilibration, and operating without highly sophisticated instruments. The results demonstrated that the eye readable colorimetric detection of glucose in levels of human blood serum could be possible by the use of these nanofibers as strips. Potentially, the same concept may be applied for the improvment of new sensors to monitor other analytes. Hence, suggested approach introduces a practical sensor development method for the detection of analytes in determined scales applicable in environmental and healthcare fields.

Declaration of competing interest

The authors declare that they have no known competing financial interests or personal relationships that could have appeared to influence the work reported in this paper.

Acknowledgments

This work was supported by Yildiz Technical University Scientific Research Projects Coordination Unit under Project Number FBA-2020-3956.

References

[1] Y. Pang, Z. Huang, Y. Yang, Y. Long, H. Zheng, Colorimetric detection of glucose based on ficin with peroxidase-like activity 189 (2018) 510–515, https://doi.org/10.1016/j.saa.2017.08.056.

[2] W.J. Zhu, D.Q. Feng, M. Chen, Z.D. Chen, R. Zhu, H.L. Fang, W. Wang, Bienzyme colorimetric detection of glucose with self-calibration based on tree-shaped paper strip, Sensors Actuators B Chem. 190 (2014) 414–418, https://doi.org/10.1016/j.snb.2013.09.007.

[3] S.H. Baek, J. Roh, C.Y. Park, M.W. Kim, R. Shi, S.K. Kailasa, T.J. Park, Cu-nanoflower decorated gold nanoparticles-graphene oxide nanofiber as electrochemical biosensor for glucose detection, Mater. Sci. Eng. C. 107 (2020), 110273, https://doi.org/10.1016/j.msec.2019.110273.

[4] C. Lu, X. Liu, Y. Li, F. Yu, L. Tang, Y. Hu, Y. Ying, Multifunctional janus hematite-silica nanoparticles: mimicking peroxidase-like activity and sensitive colorimetric detection of glucose, ACS Appl. Mater. Interfaces 7 (2015) 15395–15402, https://doi.org/10.1021/acsami.5b03423.

[5] Y. Ding, M. Chen, K. Wu, M. Chen, L. Sun, Z. Liu, Z. Shi, Q. Liu, High-performance peroxidase mimics for rapid colorimetric detection of H2O2 and glucose derived from perylene diimides functionalized Co3O4 nanoparticles, Mater. Sci. Eng. C. 80 (2017) 558–565, https://doi.org/10.1016/j.msec.2017.06.020.

[6] X. Liu, D. Huang, C. Lai, L. Qin, G. Zeng, P. Xu, B. Li, H. Yi, M. Zhang, Peroxidase-like activity of smart nanomaterials and their advanced application in colorimetric glucose biosensors, Small 15 (2019) 1–27, https://doi.org/10.1002/smll.201900133.

[7] S. Mvango, P. Mashazi, Synthesis, characterization of copper oxide-gold nanoalloys and their peroxidase-like activity towards colorimetric detection of hydrogen peroxide and glucose, Mater. Sci. Eng. C. 96 (2019) 814–823, https://doi.org/10.1016/j.msec.2018.12.010.

[8] Z. Du, C. Li, L. Li, M. Zhang, S. Xu, T. Wang, Simple fabrication of a sensitive hydrogen peroxide biosensor using enzymes immobilized in processable polyaniline nanofibers/chitosan film, Mater. Sci. Eng. C. 29 (2009) 1794–1797, https://doi.org/10.1016/j.msec.2009.02.003.

[9] M.R. Mahmoudian, W.J. Basirun, P.M. Woi, M. Sookhakian, R. Yousefi, H. Ghadimi, Y. Alias, Synthesis and characterization of Co3O4 ultra-nanosheets and Co3O4 ultra-nanosheet-Ni(OH)2 as non-enzymatic electrochemical sensors for glucose detection, Mater. Sci. Eng. C. 59 (2016) 500–508, https://doi.org/10.1016/j.msec.2015.10.055.

[10] S. Pourbeyram, J. Abdollahpour, M. Soltanpour, Green synthesis of copper oxide nanoparticles decorated reduced graphene oxide for high sensitive detection of glucose, Mater. Sci. Eng. C. 94 (2019) 850–857, https://doi.org/10.1016/j.msec.2018.10.034.

[11] R. Ayranci, B. Demirkan, B. Sen, A. Şavk, M. Ak, F. Şen, Use of the monodisperse Pt/Ni@rGO nanocomposite synthesized by ultrasonic hydroxide assisted reduction method in electrochemical nonenzymatic glucose detection, Mater. Sci. Eng. C. 99 (2019) 951–956, https://doi.org/10.1016/j.msec.2019.02.040.

[12] M. Maruthupandy, G. Rajivgandhi, T. Muneeswaran, T. Vennila, F. Quero, J. M. Song, Chitosan/silver nanocomposites for colorimetric detection of glucose molecules, Int. J. Biol. Macromol. 121 (2019) 822–828, https://doi.org/10.1016/j.ijbiomac.2018.10.063.

[13] Y. Gao, Y. Wu, J. Di, Colorimetric detection of glucose based on gold nanoparticles coupled with silver nanoparticles 173 (2017) 207–212, https://doi.org/10.1016/j.saa.2016.09.023.

[14] P.C. Lee, N.S. Li, Y.P. Hsu, C. Peng, H.W. Yang, Direct glucose detection in whole blood by colorimetric assay based on glucose oxidase-conjugated graphene oxide/MnO2 nanozymes, Analyst 144 (2019) 3038–3044, https://doi.org/10.1039/c8an02440e.

[15] M.M. Rahman, A.J.S. Ahammad, J.H. Jin, S.J. Ahn, J.J. Lee, A comprehensive review of glucose biosensors based on nanostructured metal-oxides, Sensors 10 (2010) 4855–4886, https://doi.org/10.3390/s100504855.

[16] X. Ji, Z. Su, P. Wang, G. Ma, S. Zhang, "Ready-to-use" hollow nanofiber membrane-based glucose testing strips, Analyst 139 (2014) 6467–6473, https://doi.org/10.1039/c4an01354a.

[17] Y. Xiong, Y. Zhang, P. Rong, J. Yang, W. Wang, D. Liu, A high-throughput colorimetric assay for glucose detection based on glucose oxidase-catalyzed enlargement of gold nanoparticles, Nanoscale 7 (2015) 15584–15588, https://doi.org/10.1039/c5nr03758a.

[18] P. Martinkova, R. Opatrilova, P. Kruzliak, I. Styriak, M. Pohanka, Colorimetric glucose assay based on magnetic particles having pseudo-peroxidase activity and immobilized glucose oxidase, Mol. Biotechnol. 58 (2016) 373–380, https://doi.org/10.1007/s12033-016-9936-z.

[19] E. Sapountzi, M. Braiek, J.F. Chateaux, N. Jaffrezic-Renault, F. Lagarde, Recent advances in electrospun nanofiber interfaces for biosensing devices, Sensors (Switzerland) 17 (2017), https://doi.org/10.3390/s17081887.

[20] H.C. Kim, D. Kim, J.Y. Lee, L. Zhai, J. Kim, Effect of wet spinning and stretching to enhance mechanical properties of cellulose nanofiber filament, Int. J. Precis. Eng. Manuf. 6 (2019) 567–575, https://doi.org/10.1007/s40684-019-00070-z.

[21] H. Sehaqui, N. Ezekiel Mushi, S. Morimune, M. Salajkova, T. Nishino, L. A. Berglund, Cellulose nanofiber orientation in nanopaper and nanocomposites by cold drawing, ACS Appl. Mater. Interfaces 4 (2012) 1043–1049, https://doi.org/10.1021/am2016766.

[22] P. Claro, A. de Campos, A. Corrêa, V. Rodrigues, B. Luchesi, L. Silva, G. Tonoli, L. Mattoso, J. Marconcini, Curaua and eucalyptus nanofiber films by continuous casting: mixture of cellulose nanocrystals and nanofibrils, Cellulose 26 (2019) 2453–2470, https://doi.org/10.1007/s10570-019-02280-9.

[23] Z. Dong, S.J. Kennedy, Y. Wu, Electrospinning materials for energy-related applications and devices, J. Power Sources 196 (2011) 4886–4904, https://doi.org/10.1016/j.jpowsour.2011.01.090.

[24] T. Hemamalini, V.R. Giri Dev, Comprehensive review on electrospinning of starch polymer for biomedical applications, Int. J. Biol. Macromol. 106 (2018) 712–718, https://doi.org/10.1016/j.ijbiomac.2017.08.079.

[25] J.C. Ge, J.Y. Kim, S.K. Yoon, N.J. Choi, Fabrication of low-cost and high-performance coal fly ash nanofibrous membranes via electrospinning for the control of harmful substances, Fuel 237 (2019) 236–244, https://doi.org/10.1016/j.fuel.2018.09.068.

[26] L.A. Mercante, V.P. Scagion, F.L. Migliorini, L.H.C. Mattoso, D.S. Correa, Electrospinning-based (bio)sensors for food and agricultural applications: a review, TrAC Trends Anal. Chem. 91 (2017) 91–103, https://doi.org/10.1016/j.trac.2017.04.004.

[27] B. Balusamy, A. Senthamizhan, T. Uyar, Functionalized electrospun nanofibers as colorimetric sensory probe for mercury detection: a review, Sensors (Switzerland) 19 (2019), https://doi.org/10.3390/s19214763.

[28] A. Senthamizhan, B. Balusamy, T. Uyar, Recent progress on designing electrospun nanofibers for colorimetric biosensing applications, Curr. Opin. Biomed. Eng. 13 (2020) 1–8, https://doi.org/10.1016/j.cobme.2019.08.002.

[29] J. Li, X. Liu, H. Sun, L. Wang, J. Zhang, X. Huang, L. Deng, J. Xi, T. Ma, A new type of optical fiber glucose biosensor with enzyme immobilized by electrospinning XX (2021), https://doi.org/10.1109/JSEN.2021.3075553.

[30] K. Puttananjegowda, A. Takshi, S. Thomas, Silicon carbide nanoparticles electrospun nanofibrous enzymatic glucose sensor, Biosens. Bioelectron. 186 (2021), 113285, https://doi.org/10.1016/j.bios.2021.113285.

[31] Y. Jiang, N. Song, C. Wang, N. Pinna, X. Lu, A facile synthesis of Fe3O4/nitrogen-doped carbon hybrid nanofibers as a robust peroxidase-like catalyst for the sensitive colorimetric detection of ascorbic acid, J. Mater. Chem. B 5 (2017) 5499–5505, https://doi.org/10.1039/c7tb01058c.

[32] M. Dhawane, A. Deshpande, R. Jain, P. Dandekar, Colorimetric point-of-care detection of cholesterol using chitosan nanofibers, Sensors Actuators B Chem. 281 (2019) 72–79, https://doi.org/10.1016/j.snb.2018.10.060.

[33] E.S. Ribeiro, B.S. de Farias, T.R. Sant'Anna Cadaval Junior, L.A. de Almeida Pinto, P.S. Diaz, Chitosan–based nanofibers for enzyme immobilization, Int. J. Biol. Macromol. 183 (2021) 1959–1970, https://doi.org/10.1016/j.ijbiomac.2021.05.214.

[34] N. Kutlu, Y. İspirli Doğaç, İ. Deveci, M. Teke, Urease immobilized electrospun PVA/chitosan nanofibers with improved stability and reusability characteristics: an application for removal of urea from artificial blood serum, Prep. Biochem. Biotechnol. 50 (2020) 425–437, https://doi.org/10.1080/10826068.2019.1679175.
[35] A. Morie, T. Garg, A.K. Goyal, G. Rath, Nanofibers as novel drug carrier – an overview, Artif. Cells Nanomed. Biotechnol. 44 (2016) 135–143, https://doi.org/10.3109/21691401.2014.927879.
[36] C. Reis, E. Sousa, J. Serpa, R. Oliveira, R. Oliveira, J. Santos, Design of immobilized enzyme biocatalysts: drawbacks and opportunities, Quim Nova (2019), https://doi.org/10.21577/0100-4042.20170381.
[37] E.T. Hwang, M.B. Gu, Enzyme stabilization by nano/microsized hybrid materials, Eng. Life Sci. 13 (2013) 49–61, https://doi.org/10.1002/elsc.201100225.
[38] M.M. Rahman, T.A. Sheikh, A.M. Asiri, M.R. Awual, Development of 3-methoxyaniline sensor probe based on thin ag 2 O@La 2 O 3 nanosheets for environmental safety, New J. Chem. 43 (2019) 4620–4632, https://doi.org/10.1039/C9NJ00415G.
[39] M.M. Alam, A.M. Asiri, M.T. Uddin, M.A. Islam, M.R. Awual, M.M. Rahman, Detection of uric acid based on doped ZnO/Ag2O/Co3O4 nanoparticle loaded glassy carbon electrode, New J. Chem. 43 (2019) 8651–8659, https://doi.org/10.1039/C9NJ01287G.
[40] M.M. Rahman, M.M. Hussain, M.N. Arshad, M.R. Awual, A.M. Asiri, Arsenic sensor development based on modification with (E)- N ′-(2-nitrobenzylidine)-benzenesulfonohydrazide: a real sample analysis, New J. Chem. 43 (2019) 9066–9075, https://doi.org/10.1039/C9NJ01567A.
[41] R.M. Kamel, A. Shahat, W.H. Hegazy, E.M. Khodier, M.R. Awual, Efficient toxic nitrite monitoring and removal from aqueous media with ligand based conjugate materials, J. Mol. Liq. 285 (2019) 20–26, https://doi.org/10.1016/j.molliq.2019.04.060.
[42] S. Khandaker, Y. Toyohara, G.C. Saha, M.R. Awual, T. Kuba, Development of synthetic zeolites from bio-slag for cesium adsorption: kinetic, isotherm and thermodynamic studies, J. Water Process Eng. 33 (2020), 101055, https://doi.org/10.1016/j.jwpe.2019.101055.
[43] M.R. Awual, T. Yaita, T. Kobayashi, H. Shiwaku, S. Suzuki, Improving cesium removal to clean-up the contaminated water using modified conjugate material, J. Environ. Chem. Eng. 8 (2020), 103684, https://doi.org/10.1016/j.jece.2020.103684.
[44] M.R. Awual, M.M. Hasan, J. Iqbal, A. Islam, M.A. Islam, A.M. Asiri, M. M. Rahman, Naked-eye lead(II) capturing from contaminated water using innovative large-pore facial composite materials, Microchem. J. 154 (2020), 104585, https://doi.org/10.1016/j.microc.2019.104585.
[45] M.R. Awual, M.M. Hasan, J. Iqbal, M.A. Islam, A. Islam, S. Khandaker, A.M. Asiri, M.M. Rahman, Ligand based sustainable composite material for sensitive nickel (II) capturing in aqueous media, J. Environ. Chem. Eng. 8 (2020), 103591, https://doi.org/10.1016/j.jece.2019.103591.
[46] T.A. Sheikh, M.M. Rahman, A.M. Asiri, H.M. Marwani, M.R. Awual, 4-hexylresorcinol sensor development based on wet-chemically prepared Co3O4@Er2O3 nanorods: a practical approach, J. Ind. Eng. Chem. 66 (2018) 446–455, https://doi.org/10.1016/j.jiec.2018.06.012.
[47] C. Li, Y. Su, X. Lv, H. Xia, H. Shi, X. Yang, J. Zhang, Y. Wang, Controllable anchoring of gold nanoparticles to polypyrrole nanofibers by hydrogen bonding and their application in nonenzymatic glucose sensors, Biosens. Bioelectron. 38 (2012) 402–406, https://doi.org/10.1016/j.bios.2012.04.049.
[48] Y. Ding, Y. Wang, L. Su, H. Zhang, Y. Lei, Preparation and characterization of NiO-Ag nanofibers, NiO nanofibers, and porous Ag: towards the development of a highly sensitive and selective non-enzymatic glucose sensor, J. Mater. Chem. 20 (2010) 9918–9926, https://doi.org/10.1039/c0jm01968b.
[49] Y. Liu, H. Teng, H. Hou, T. You, Nonenzymatic glucose sensor based on renewable electrospun ni nanoparticle-loaded carbon nanofiber paste electrode, Biosens. Bioelectron. 24 (2009) 3329–3334, https://doi.org/10.1016/j.bios.2009.04.032.
[50] P. Naderi Asrami, M. Saber Tehrani, P. Aberoomand Azar, S.A. Mozaffari, Impedimetric glucose biosensor based on nanostructure nickel oxide transducer fabricated by reactive RF magnetron sputtering system, J. Electroanal. Chem. 801 (2017) 258–266, https://doi.org/10.1016/j.jelechem.2017.07.052.
[51] P. Naderi Asrami, S.A. Mozaffari, M. Saber Tehrani, P. Aberoomand Azar, A novel impedimetric glucose biosensor based on immobilized glucose oxidase on a CuO-chitosan nanobiocomposite modified FTO electrode, Int. J. Biol. Macromol. 118 (2018) 649–660, https://doi.org/10.1016/j.ijbiomac.2018.05.228.
[52] S. Khazaei, S.A. Mozaffari, F. Ebrahimi, Polyvinyl alcohol as a crucial omissible polymer to fabricate an impedimetric glucose biosensor based on hierarchical 3D-NPZnO/chitosan, Carbohydr. Polym. 266 (2021), 118105, https://doi.org/10.1016/j.carbpol.2021.118105.
[53] T. Gunnlaugsson, P.E. Kruger, P. Jensen, J. Tierney, H.D.P. Ali, G.M. Hussey, Colorimetric "Naked eye" sensing of anions in aqueous solution, J. Org. Chem. 70 (2005) 10875–10878, https://doi.org/10.1021/jo0520487.
[54] X. Liu, H.T. Ngo, Z. Ge, S.J. Butler, K.A. Jolliffe, Tuning colourimetric indicator displacement assays for naked-eye sensing of pyrophosphate in aqueous media, Chem. Sci. 4 (2013) 1680, https://doi.org/10.1039/c3sc22233k.
[55] P. Bösiger, G. Tegl, I.M.T. Richard, L. Le Gat, L. Huber, V. Stagl, A. Mensah, G. M. Guebitz, R.M. Rossi, G. Fortunato, Enzyme functionalized electrospun chitosan mats for antimicrobial treatment, Carbohydr. Polym. 181 (2018) 551–559, https://doi.org/10.1016/j.carbpol.2017.12.002.
[56] T.E. Herricks, S.-H. Kim, J. Kim, D. Li, J.H. Kwak, J.W. Grate, S.H. Kim, Y. Xia, Direct fabrication of enzyme-carrying polymer nanofibers by electrospinning, J. Mater. Chem. 15 (2005) 3241, https://doi.org/10.1039/b503660g.
[57] R.-S. Juang, F.-C. Wu, R.-L. Tseng, Use of chemically modified chitosan beads for sorption and enzyme immobilization, Adv. Environ. Res. 6 (2002) 171–177, https://doi.org/10.1016/S1093-0191(00)00078-2.
[58] Y. Tao, Y. Zhang, Y. Cheng, Y. Wang, Rapid screening and identification of α -glucosidase inhibitors from mulberry leaves using enzyme-immobilized magnetic beads coupled with HPLC/MS and NMR, Biomed. Chromatogr. 27 (2013) 148–155, https://doi.org/10.1002/bmc.2761.
[59] M.A. Burns, G.I. Kvesitadze, D.J. Graves, Dried calcium alginate/magnetite spheres: a new support for chromatographic separations and enzyme immobilization, Biotechnol. Bioeng. 27 (1985) 137–145, https://doi.org/10.1002/bit.260270206.
[60] I. Benucci, K. Liburdi, I. Cacciotti, C. Lombardelli, M. Zappino, F. Nanni, M. Esti, Chitosan/clay nanocomposite films as supports for enzyme immobilization: an innovative green approach for winemaking applications, Food Hydrocoll. 74 (2018) 124–131, https://doi.org/10.1016/j.foodhyd.2017.08.005.
[61] S. Xu, Y. Liu, W. Zhao, Q. Wu, Y. Chen, X. Huang, Z. Sun, Y. Zhu, X. Liu, Hierarchical 0D–2D bio-composite film based on enzyme-loaded polymeric nanoparticles decorating graphene nanosheets as a high-performance bio-sensing platform, Biosens. Bioelectron. 156 (2020), 112134, https://doi.org/10.1016/j.bios.2020.112134.
[62] B.S. de Farias, T.R. Sant'Anna Cadaval Junior, L.A. de Almeida Pinto, Chitosan-functionalized nanofibers: a comprehensive review on challenges and prospects for food applications, Int. J. Biol. Macromol. 123 (2019) 210–220, https://doi.org/10.1016/j.ijbiomac.2018.11.042.
[63] B.S. de Farias, D.D.R. Gründmann, M.M. Strieder, N. da Silveira, T.R.S. Cadaval, L.A. de Almeida Pinto, Biosorption of glycerol impurities from biodiesel production onto electrospun chitosan-based nanofibers: equilibrium and thermodynamic evaluations, Environ. Sci. Pollut. Res. 26 (2019) 28436–28443, https://doi.org/10.1007/s11356-019-04525-3.
[64] M. Sharifi, M.J. Sohrabi, S.H. Hosseinali, A. Hasan, P.H. Kani, A.J. Talaei, A. Y. Karim, N.M.Q. Nanakali, A. Salihi, F.M. Aziz, B. Yan, R.H. Khan, A.A. Saboury, M. Falahati, Enzyme immobilization onto the nanomaterials: application in enzyme stability and prodrug-activated cancer therapy, Int. J. Biol. Macromol. 143 (2020) 665–676, https://doi.org/10.1016/j.ijbiomac.2019.12.064.
[65] A.R. Ismail, K.-H. Baek, Lipase immobilization with support materials, preparation techniques, and applications: present and future aspects, Int. J. Biol. Macromol. 163 (2020) 1624–1639, https://doi.org/10.1016/j.ijbiomac.2020.09.021.
[66] J. Maitra, V.K. Shukla, Cross-linking in hydrogels - a review, Am. J. Polym. Sci. 4 (2014) 25–31, https://doi.org/10.5923/j.ajps.20140402.01.
[67] A. Naeimi, M. Payandeh, A.R. Ghara, F.E. Ghadi, In vivo evaluation of the wound healing properties of bio-nanofiber chitosan/polyvinyl alcohol incorporating honey and nepeta dschuparensis, Carbohydr. Polym. 240 (2020), 116315, https://doi.org/10.1016/j.carbpol.2020.116315.
[68] P. Agrawal, K. Pramanik, Tissue Eng.Regen. Med. 13 (2016) 485–497, https://doi.org/10.1007/s13770-016-9092-3.
[69] N. Bhattarai, Nanofibrous structure of chitosan for biomedical applications, J. Nanomed. Biother. Discov. 02 (2012) 1–9, https://doi.org/10.4172/2155-983x.1000102.
[70] M. Koosha, H. Mirzadeh, Electrospinning, mechanical properties, and cell behavior study of chitosan/PVA nanofibers, J. Biomed. Mater. Res.A. 103 (2015) 3081–3093, https://doi.org/10.1002/jbm.a.35443.
[71] R. Ahmed, M. Tariq, I. Ali, R. Asghar, P. Noorunnisa Khanam, R. Augustine, A. Hasan, Novel electrospun chitosan/polyvinyl alcohol/zinc oxide nanofibrous mats with antibacterial and antioxidant properties for diabetic wound healing, Int. J. Biol. Macromol. 120 (2018) 385–393, https://doi.org/10.1016/j.ijbiomac.2018.08.057.
[72] S.P. Rwei, C.C. Huang, Electrospinning PVA solution-rheology and morphology analyses, Fibers Polym. 13 (2012) 44–50, https://doi.org/10.1007/s12221-012-0044-9.
[73] M. Mozafari, Jalali Moztarzadeh, N. Alhosseini, Dodel Asgari, Kargozar Samadikuchaksaraei, Synthesis and characterization of electrospun polyvinyl alcohol nanofibrous scaffolds modified by blending with chitosan for neural tissue engineering, Int. J. Nanomedicine (2012) 25, https://doi.org/10.2147/ijn.s25376.
[74] H. Adeli, M.T. Khorasani, M. Parvazinia, Wound dressing based on electrospun PVA/chitosan/starch nanofibrous mats: fabrication, antibacterial and cytocompatibility evaluation and in vitro healing assay, Int. J. Biol. Macromol. 122 (2019) 238–254, https://doi.org/10.1016/j.ijbiomac.2018.10.115.
[75] A.M. Abdelgawad, M.E. El-Naggar, S.M. Hudson, O.J. Rojas, Fabrication and characterization of bactericidal thiol-chitosan and chitosan iodoacetamide nanofibres, Int. J. Biol. Macromol. 94 (2017) 96–105, https://doi.org/10.1016/j.ijbiomac.2016.07.061.
[76] T.T. Li, M. Yan, Y. Zhong, H.T. Ren, C.W. Lou, S.Y. Huang, J.H. Lin, Processing and characterizations of rotary linear needleless electrospun polyvinyl alcohol (PVA)/Chitosan(CS)/Graphene(Gr) nanofibrous membranes, J. Mater. Res. Technol. 8 (2019) 5124–5132, https://doi.org/10.1016/j.jmrt.2019.08.035.
[77] V.S. Waghmare, P.R. Wadke, S. Dyawanapelly, A. Deshpande, R. Jain, P. Dandekar, Starch based nanofibrous scaffolds for wound healing applications, Bioact. Mater. 3 (2018) 255–266, https://doi.org/10.1016/j.bioactmat.2017.11.006.
[78] S.R. Gomes, G. Rodrigues, G.G. Martins, M.A. Roberto, M. Mafra, C.M. R. Henriques, J.C. Silva, In vitro and in vivo evaluation of electrospun nanofibers of PCL, chitosan and gelatin: a comparative study, Mater. Sci. Eng. C. 46 (2015) 348–358, https://doi.org/10.1016/j.msec.2014.10.051.

[79] N. Dorraki, N.N. Safa, M. Jahanfar, H. Ghomi, S.O. Ranaei-Siadat, Surface modification of chitosan/PEO nanofibers by air dielectric barrier discharge plasma for acetylcholinesterase immobilization, Appl. Surf. Sci. 349 (2015) 940–947, https://doi.org/10.1016/j.apsusc.2015.03.118.
[80] V.A. Pereira, I.N.Q. de Arruda, R. Stefani, Active chitosan/PVA films with anthocyanins from Brassica oleraceae (red cabbage) as time-temperature indicators for application in intelligent food packaging, Food Hydrocoll. 43 (2015) 180–188, https://doi.org/10.1016/j.foodhyd.2014.05.014.
[81] I.M. Jipa, A. Stoica, M. Stroescu, L.M. Dobre, T. Dobre, S. Jinga, C. Tardei, Potassium sorbate release from poly(vinyl alcohol)-bacterial cellulose films, Chem. Pap. 66 (2012) 138–143, https://doi.org/10.2478/s11696-011-0068-4.
[82] Z. Cui, Z. Zheng, L. Lin, J. Si, Q. Wang, X. Peng, W. Chen, Electrospinning and crosslinking of polyvinyl alcohol/chitosan composite nanofiber for transdermal drug delivery, Adv. Polym. Technol. 37 (2018) 1917–1928, https://doi.org/10.1002/adv.21850.
[83] I.Y. Prosanov, A.A. Matvienko, Study of PVA thermal destruction by means of IR and raman spectroscopy, Phys. Solid State 52 (2010) 2203–2206, https://doi.org/10.1134/S1063783410100318.
[84] X.D. Ren, Q.S. Liu, H. Feng, X.Y. Yin, The characterization of chitosan nanoparticles by raman spectroscopy, Appl. Mech. Mater. 665 (2014) 367–370, https://doi.org/10.4028/www.scientific.net/AMM.665.367.
[85] N.L.G.D. Souza, T.F. Salles, H.M. Brandão, H.G.M. Edwards, L.F.C. De Oliveira, Synthesis, vibrational spectroscopic and thermal properties of oxocarbon cross-linked chitosan, J. Braz. Chem. Soc. 26 (2015) 1247–1256, https://doi.org/10.5935/0103-5053.20150090.
[86] E. Szymańska, K. Winnicka, Stability of chitosan - a challenge for pharmaceutical and biomedical applications, Mar. Drugs 13 (2015) 1819–1846, https://doi.org/10.3390/md13041819.
[87] K. Triyana, M.S. Mu'Min, K. Faizah, Y. Yusuf, A. Kusumaatmaja, Harsojo, Electrospun nanofibers based on polyvinyl alcohol/chitosan and its stability in KOH solution, Mater. Sci. Forum. 827 (2015) 321–325.
[88] W.A. Sarhan, H.M.E. Azzazy, I.M. El-Sherbiny, The effect of increasing honey concentration on the properties of the honey/polyvinyl alcohol/chitosan nanofibers, Mater. Sci. Eng. C. 67 (2016) 276–284, https://doi.org/10.1016/j.msec.2016.05.006.
[89] M. Altikatoglu, Y. Basaran, C. Arioz, A. Ogan, H. Kuzu, Glucose oxidase-dextran conjugates with enhanced stabilities against temperature and pH, Appl. Biochem. Biotechnol. 160 (2010) 2187–2197, https://doi.org/10.1007/s12010-009-8812-8.
[90] X. Luo, J. Xia, X. Jiang, M. Yang, S. Liu, Cellulose-based strips designed based on a sensitive enzyme colorimetric assay for the low concentration of glucose detection, Anal. Chem. 91 (2019) 15461–15468, https://doi.org/10.1021/acs.analchem.9b03180.
[91] S. Demirci Uzun, F. Kayaci, T. Uyar, S. Timur, L. Toppare, Bioactive surface design based on functional composite electrospun nanofibers for biomolecule immobilization and biosensor applications, ACS Appl.Mater. Interfaces 6 (2014) 5235–5243, https://doi.org/10.1021/am5005927.
[92] E.F.M. Gabriel, P.T. Garcia, F.M. Lopes, W.K.T. Coltro, Paper-based colorimetric biosensor for tear glucose measurements, Micromachines. 8 (2017) 1–9, https://doi.org/10.3390/mi8040104.
[93] M. Li, L. Liu, Y. Xiong, X. Liu, A. Nsabimana, X. Bo, L. Guo, Bimetallic MCo (M = cu, fe, ni, and Mn) nanoparticles doped-carbon nanofibers synthetized by electrospinning for nonenzymatic glucose detection, Sensors Actuators B Chem. 207 (2015) 614–622, https://doi.org/10.1016/j.snb.2014.10.092.
[94] M. Raicopol, A. Prună, C. Damian, L. Pilan, Functionalized single-walled carbon nanotubes/polypyrrole composites for amperometric glucose biosensors, Nanoscale Res. Lett. 8 (2013) 1–8, https://doi.org/10.1186/1556-276X-8-316.
[95] C. Zhou, Y. Shi, X. Ding, M. Li, J. Luo, Z. Lu, D. Xiao, Development of a fast and sensitive glucose biosensor using iridium complex-doped electrospun optical fibrous membrane, Anal. Chem. 85 (2013) 1171–1176, https://doi.org/10.1021/ac303107d.
[96] E.F. O'Connor, S. Paterson, R. de la Rica, Naked-eye detection as a universal approach to lower the limit of detection of enzyme-linked immunoassays, Anal. Bioanal. Chem. 408 (2016) 3389–3393, https://doi.org/10.1007/s00216-016-9453-8.
[97] N. Wu, L.-X. Zhao, C.-Y. Jiang, P. Li, Y. Liu, Y. Fu, F. Ye, A naked-eye visible colorimetric and fluorescent chemosensor for rapid detection of fluoride anions: implication for toxic fluorine-containing pesticides detection, J. Mol. Liq. 302 (2020), 112549, https://doi.org/10.1016/j.molliq.2020.112549.
[98] V. Kovida, A.L. Sharma, Koner, rapid on-site and naked-eye detection of common nitro pesticides with ionic liquids, Analyst 145 (2020) 4335–4340, https://doi.org/10.1039/D0AN00452A.
[99] H. Ma, K. Song, L. Zhou, X. Zhao, A naked eye refractive index sensor with a visible multiple peak metamaterial absorber, Sensors 15 (2015) 7454–7461, https://doi.org/10.3390/s150407454.
[100] P.M. Castillo, F.J. Fernández-Acejo, J.M. Carnerero, R. Prado-Gotor, A. Jimenez-Ruiz, Colorimetric, naked-eye detection of lysozyme in human urine with gold nanoparticles, Nanomaterials 11 (2021) 612, https://doi.org/10.3390/nano11030612.
[101] L. Santana-Jiménez, A. Márquez-Lucero, V. Osuna, I. Estrada-Moreno, R. Dominguez, Naked-eye detection of glucose in saliva with bienzymatic paper-based sensor, Sensors 18 (2018) 1071, https://doi.org/10.3390/s18041071.
[102] N.V. Saranchina, A.A. Dudkina, M.M. Gavrilenko, N.A. Gavrilenko, A simple method for colorimetric and naked-eye detection of mercury in fish products, Mater. Sci. Forum 970 (2019) 219–226, https://doi.org/10.4028/www.scientific.net/MSF.970.219.
[103] C. Radhakumary, K. Sreenivasan, Naked eye detection of glucose in urine using glucose oxidase immobilized gold nanoparticles, Anal. Chem. 83 (2011) 2829–2833, https://doi.org/10.1021/ac1032879.
[104] Y. Lin, M. Zhao, Y. Guo, X. Ma, F. Luo, L. Guo, B. Qiu, G. Chen, Z. Lin, Multicolor colormetric biosensor for the determination of glucose based on the etching of gold nanorods, Sci. Rep. 6 (2016) 37879, https://doi.org/10.1038/srep37879.
[105] Z.F. Gao, E.E. Sann, X. Lou, R. Liu, J. Dai, X. Zuo, F. Xia, L. Jiang, Naked-eye point-of-care testing platform based on a pH-responsive superwetting surface: toward the non-invasive detection of glucose, NPG Asia Mater. 10 (2018) 177–189, https://doi.org/10.1038/s41427-018-0024-7.
[106] X. Wu, J. Yin, J. Liu, Y. Gu, S. Wang, J. Wang, Colorimetric detection of glucose based on the binding specificity of a synthetic cyclic peptide, Analyst 145 (2020) 7234–7241, https://doi.org/10.1039/D0AN00211A.
[107] L.T. Nguyen, K.-L. Yang, Combined cross-linked enzyme aggregates of horseradish peroxidase and glucose oxidase for catalyzing cascade chemical reactions, Enzym. Microb. Technol. 100 (2017) 52–59, https://doi.org/10.1016/j.enzmictec.2017.02.007.
[108] D.E. Goldstein, R.R. Little, R.A. Lorenz, J.I. Malone, D. Nathan, C.M. Peterson, D. B. Sacks, Tests of glycemia in diabetes, Diabetes Care 27 (2004) 1761–1773, https://doi.org/10.2337/diacare.27.7.1761.
[109] J.-L. Lin, L. Palomec, I. Wheeldon, Design and analysis of enhanced catalysis in scaffolded multienzyme cascade reactions, ACS Catal. 4 (2014) 505–511, https://doi.org/10.1021/cs401009z.
[110] J. Müller, C.M. Niemeyer, DNA-directed assembly of artificial multienzyme complexes, Biochem. Biophys. Res. Commun. 377 (2008) 62–67, https://doi.org/10.1016/j.bbrc.2008.09.078.
[111] E.W. Stein, D.V. Volodkin, M.J. McShane, G.B. Sukhorukov, Real-time assessment of spatial and temporal coupled catalysis within polyelectrolyte microcapsules containing coimmobilized glucose oxidase and peroxidase, Biomacromolecules 7 (2006) 710–719, https://doi.org/10.1021/bm050304j.
[112] J. Fu, M. Liu, Y. Liu, N.W. Woodbury, H. Yan, Interenzyme substrate diffusion for an enzyme Cascade organized on spatially addressable DNA nanostructures, J. Am. Chem. Soc. 134 (2012) 5516–5519, https://doi.org/10.1021/ja300897h.
[113] Y. Fu, D. Zeng, J. Chao, Y. Jin, Z. Zhang, H. Liu, D. Li, H. Ma, Q. Huang, K. V. Gothelf, C. Fan, Single-step rapid assembly of DNA origami nanostructures for addressable nanoscale bioreactors, J. Am. Chem. Soc. 135 (2013) 696–702, https://doi.org/10.1021/ja3076692.